Published Online: 21 May, 2012 | Supp Info: http://doi.org/10.1083/jcb.201203065

Basement membrane assembly of the integrin α8β1 ligand nephronectin requires Fraser syndrome–associated proteins

Daiji Kiyozumi,[1] Makiko Takeichi,[1] Itsuko Nakano,[1] Yuya Sato,[1] Tomohiko Fukuda,[2] and Kiyotoshi Sekiguchi[1]

[1]Laboratory of Extracellular Matrix Biochemistry, Institute for Protein Research, Osaka University, Suita, Osaka 565-0871, Japan
[2]Sekiguchi Biomatrix Signaling Project, Japan Science and Technology Agency, Aichi Medical University, Nagakute, Aichi 480-1195, Japan

Dysfunction of the basement membrane protein QBRICK provokes Fraser syndrome, which results in renal dysmorphogenesis, cryptophthalmos, syndactyly, and dystrophic epidermolysis bullosa through unknown mechanisms. Here, we show that integrin α8β1 binding to basement membranes was significantly impaired in *Qbrick*-null mice. This impaired integrin α8β1 binding was not a direct consequence of the loss of QBRICK, which itself is a ligand of integrin α8β1, because knock-in mice with a mutation in the integrin-binding site of QBRICK developed normally and do not exhibit any defects in integrin α8β1 binding. Instead, the loss of QBRICK significantly diminished the expression of nephronectin, an integrin α8β1 ligand necessary for renal development. In vivo, nephronectin associated with QBRICK and localized at the sublamina densa region, where QBRICK was also located. Collectively, these findings indicate that QBRICK facilitates the integrin α8β1–dependent interactions of cells with basement membranes by regulating the basement membrane assembly of nephronectin and explain why renal defects occur in Fraser syndrome.

Introduction

Fraser syndrome (FS) is a rare autosomal recessive multiorgan disorder characterized by cryptophthalmos, syndactyly, renal agenesis, and a variety of morphogenetic defects (Slavotinek and Tifft, 2002). Approximately 45% of human cases are stillborn or die within the first year, primarily from pulmonary and/or renal complications (Boyd et al., 1988). Based on the phenotypic similarities, a group of mutant mice, called blebbing mice, are considered to be animal models of human FS (Darling and Gossler, 1994). Blebbing mice are characterized by epidermal blistering, classified as dystrophic epidermolysis bullosa, during the embryonic period and exhibit FS-like developmental defects, including cryptophthalmos, syndactyly, and renal agenesis (Darling and Gossler, 1994).

The molecular basis of FS had long been unknown until causative mutations were identified in FS patients and blebbing mice. Four genes encoding Fras1, Frem2, QBRICK (also named Frem1), and Grip1 have been found to be disrupted in FS patients and/or blebbing mice (Bladt et al., 2002; McGregor et al., 2003; Vrontou et al., 2003; Smyth et al., 2004; Takamiya et al., 2004; Jadeja et al., 2005; Timmer et al., 2005; Kiyozumi et al., 2006; Alazami et al., 2009). Among these gene products, QBRICK, Fras1, and Frem2 are members of a novel family of ECM proteins characterized by 12 consecutive CSPG repeats and a varying number of Calx-β domains. Fras1 and Frem2 are produced by epithelial cells as membrane proteins with a short C-terminal tail containing a PDZ domain-binding motif (McGregor et al., 2003; Vrontou et al., 2003; Jadeja et al., 2005; Timmer et al., 2005) and secreted after proteolytic processing near the juxtamembrane region (Kiyozumi et al., 2006; Carney et al., 2010). In contrast, QBRICK is produced by mesenchymal cells as a secreted protein (Smyth et al., 2004; Kiyozumi et al., 2006). These three proteins meet together at the basement membrane (BM) zone between the epithelial and mesenchymal tissues and reciprocally stabilize one another by forming a ternary complex. When any one of these proteins is lost or truncated, the other proteins fail to

Correspondence to Kiyotoshi Sekiguchi: sekiguch@protein.osaka-u.ac.jp

Tomohiko Fukuda's present address is Division of Regulatory Glycobiology, Institute of Molecular Biomembrane and Glycobiology, Tohoku Pharmaceutical University, Sendai, Miyagi 988-8558, Japan.

Abbreviations used in this paper: BM, basement membrane; FS, Fraser syndrome; GDNF, glial cell line-derived neurotrophic factor.

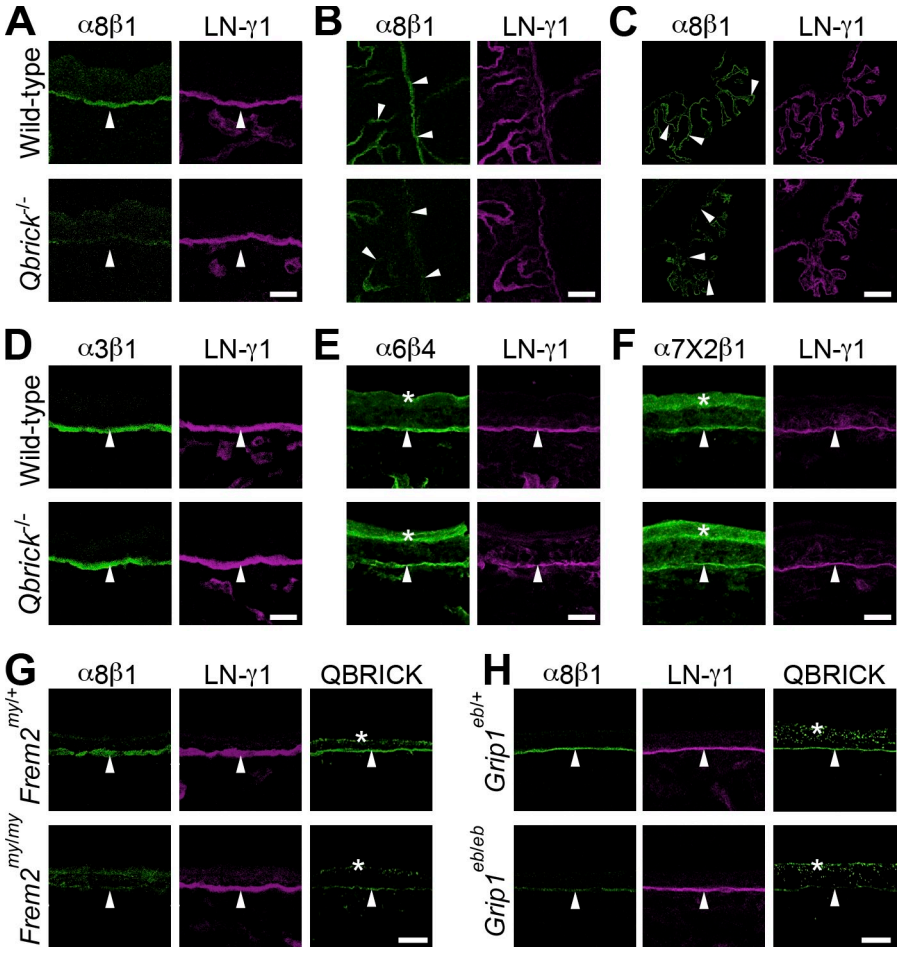

Figure 1. **In situ binding of recombinant integrins to frozen sections of mouse embryonic tissues.** (A–C) Recombinant integrin α8β1 (green) bound to E15.5 dorsal skin (A), lung (B), and choroid plexus (C) cryosections. The top and bottom panels show fluorescence images for wild-type and *Qbrick*$^{-/-}$ littermates, respectively. (D–F) Integrins α3β1 (D), α6β4 (E), and α7X2β1 (F) bound to dorsal skin cryosections from wild-type (top) and *Qbrick*$^{-/-}$ (bottom) littermates were visualized (green). (G and H) Integrin α8β1 (green) bound to dorsal skin cryosections from *Frem2*$^{my/+}$ and *Frem2*$^{my/my}$ (G) and *Grip1*$^{eb/+}$ and *Grip1*$^{eb/eb}$ (H) mice. The top and bottom panels show fluorescence images for control heterozygotes and homozygotes, respectively. The BMs were counterstained with an anti–laminin-γ1 chain antibody (magenta). Immunoreactivity against QBRICK (green) is also shown. Arrowheads indicate the location of BMs. The asterisks indicate nonspecific binding of recombinant integrins or the anti-QBRICK antibody to the cornified epithelium. Bars, 20 µm.

stably localize at BMs (Kiyozumi et al., 2006). Grip1 is an intracellular adaptor protein that contains multiple PDZ domains, with which it binds to Fras1 and Frem2 (Takamiya et al., 2004). Dysfunction of Grip1 impairs the secretion of Fras1 (Takamiya et al., 2004) and results in the breakdown of the ternary complex between the three FS-associated proteins (Kiyozumi et al., 2006).

Although the reciprocal stabilization of QBRICK, Fras1, and Frem2 is apparently indispensable, it remains elusive how these molecules operate at BMs to regulate organ development. Little is known about the biochemical functions of QBRICK, Fras1, and Frem2, except that QBRICK has an Arg-Gly-Asp (RGD) integrin-binding motif and is capable of mediating cell adhesion that is dependent on RGD-binding integrins such as α8β1 (Kiyozumi et al., 2005). It has been shown that integrin α8β1 ligands are expressed at embryonic BMs and play important roles in organogenetic processes involving epithelial–mesenchymal interactions. For example, nephronectin, a BM protein that binds to integrin α8β1, has been shown to play a pivotal role in kidney morphogenesis, as nephronectin-deficient mice frequently exhibit renal agenesis or hypoplasia (Linton et al., 2007). Mice deficient in integrin α8β1 expression also display severe defects in kidney morphogenesis (Müller et al., 1997). Given that renal agenesis is one of the typical phenotypes of FS and its model animals and that QBRICK is an RGD-containing ligand for integrin α8β1, some of the developmental defects associated with FS may result from loss of QBRICK from BMs as an integrin α8β1 ligand.

In this study, we investigated the role of QBRICK in the pathogenesis of FS by addressing its potential role as an integrin α8β1 ligand at embryonic BMs. Our data indicate that ablation of QBRICK expression significantly reduces the ability of BMs to interact with integrin α8β1, despite the fact that QBRICK does not account per se for the reduced integrin α8β1 binding. Instead, QBRICK is necessary for the BM assembly of nephronectin, another integrin α8β1 ligand critical for renal development. Our findings shed light on the hitherto unknown mechanism that defines the ability of BMs to interact with integrin α8β1 through the coordinated assembly of RGD-containing integrin ligands beneath the embryonic BMs.

Results

QBRICK is necessary for embryonic BMs to interact with integrin α8β1

To examine whether loss of QBRICK affects the ability of BMs to interact with integrin α8β1, we performed in situ integrin binding assays in which recombinant soluble forms of integrins were incubated with frozen sections of mouse embryos to visualize the integrin binding activities in tissues. Recombinant integrin α8β1 bound to various organs in E15.5 embryos, including the skin, lung, and choroid plexus, where the bound integrins

were localized at BMs and colocalized with immunoreactivity for laminin-γ1 (Fig. 1, A–C). The binding of integrin α8β1 in situ was abolished by adding EDTA or GRGDSP peptide, but not by adding GRGESP peptide (unpublished data), confirming that the binding was divalent ion–dependent and therefore intrinsic to the ligand-binding activity of integrin α8β1. In *Qbrick*$^{-/-}$ embryos, however, the integrin α8β1 binding to BMs was greatly reduced compared with wild-type littermates (Fig. 1, A–C).

To clarify whether the impaired integrin binding was specific to the α8β1 isoform, we performed in situ binding assays with integrin α3β1, which binds to laminin-511 and laminin-332, the major laminin isoforms of epidermal BMs (Nishiuchi et al., 2006). Integrin α3β1 bound to the BMs of both wild-type and *Qbrick*$^{-/-}$ embryos, and showed no significant difference between them (Fig. 1 D). Similarly, as shown in Fig. 1 (E and F), the BMs in *Qbrick*$^{-/-}$ embryos remained unaffected with respect to their abilities to bind integrins α6β4 and α7X2β1, other laminin-binding integrins with distinct ligand specificities (Nishiuchi et al., 2006). These findings indicate that the integrin α8β1 binding ability is specifically deprived from BMs by ablation of QBRICK.

Next, we investigated whether the impaired binding of integrin α8β1 coincides with the attenuated expression of QBRICK in other FS model animals. We investigated *Grip1* mutant *Grip1*^{eb} and *Frem2* mutant *Frem2*^{my} mice, both of which exhibit attenuated expression of QBRICK at BMs (Kiyozumi et al., 2006). In both types of mutant embryos, the binding of integrin α8β1 to BMs was significantly reduced in the epidermis (Fig. 1, G and H), which is consistent with the diminished expression of QBRICK at BMs (Fig. 1, G and H). These findings indicate that the impaired ability of BMs to bind integrin α8β1 coincides with the attenuated expression of QBRICK irrespective of the causative mutation.

Although integrin α8β1 is broadly expressed, it has a critical function in kidney development (Müller et al., 1997). Because renal dysmorphogenesis is one of the developmental defects observed in FS animals (Fig. 2 A; Darling and Gossler, 1994), we reexamined the occurrence of renal dysmorphogenesis in *Qbrick*$^{-/-}$ mice, and found that >90% of *Qbrick*$^{-/-}$ mice exhibited renal defects; i.e., 10 unilateral renal agenesis and two unilateral or bilateral renal dysgenesis among 13 E15.5 embryos, demonstrating a close association of renal agenesis with QBRICK deficiency. Therefore, we examined the integrin α8β1 binding activities of the BMs in the developing kidneys of *Qbrick*$^{-/-}$ embryos. Metanephric development starts by budding of a ureteric bud from the mesonephric duct at around embryonic day 11.5 (E11.5). The metanephric mesenchyme interacts with the ureteric bud BM through integrin α8β1 (Müller et al., 1997). In wild-type embryos, integrin α8β1 bound to the BMs of the mesonephric duct and ureteric bud (Fig. 2, B and C), where QBRICK was also expressed (Fig. 2, D and E). In the kidney of *Qbrick*$^{-/-}$ littermates, however, the integrin binding was greatly diminished (Fig. 2, B and C).

Glial cell line-derived neurotrophic factor (GDNF), a critical nephrogenic factor (Moore et al., 1996; Pichel et al., 1996; Sánchez et al., 1996), has been shown to require integrin α8β1–dependent interactions of the metanephric mesenchyme with the BMs of the ureteric buds during metanephric development (Linton et al., 2007). We investigated whether the *Qbrick*$^{-/-}$ metanephros was associated with reduced expression of *Gdnf* by quantitative RT-PCR analysis. The expression of *Gdnf* was

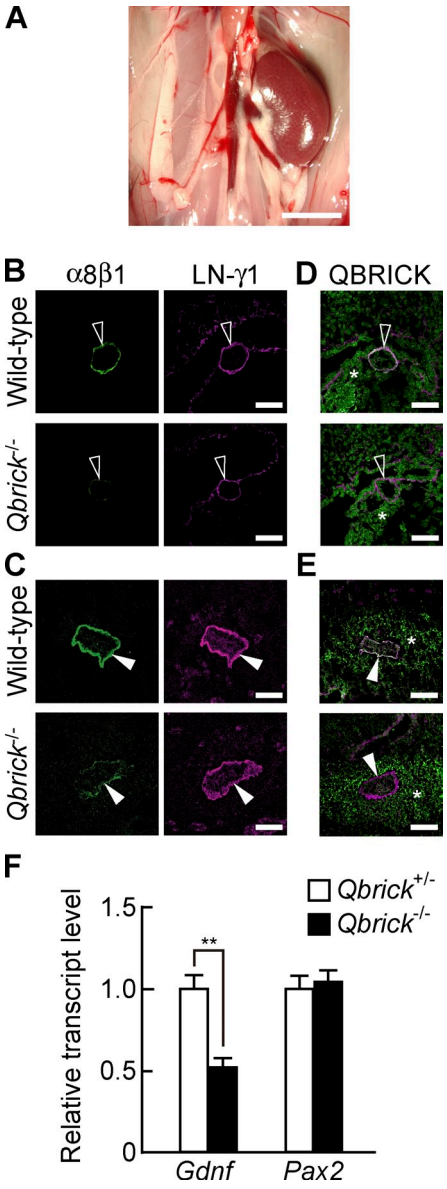

Figure 2. **Impaired binding of integrin α8β1 in the developing kidney of *Qbrick*$^{-/-}$ mice.** (A) Unilateral renal agenesis observed in *Qbrick*$^{-/-}$ mice. Bar, 5 mm. (B and C) The left panels show integrin α8β1 (green) bound to the BMs of the E10.5 mesonephric duct (B) and E11.5 ureteric bud (C) of wild-type (top) and *Qbrick*$^{-/-}$ (bottom) embryos. The right panels show the BMs counterstained with an anti–laminin-γ1 chain antibody (magenta). (D and E) QBRICK immunofluorescence (green) in the developing kidney of wild-type (top) and *Qbrick*$^{-/-}$ (bottom) embryos at E10.5 (D) and E11.5 (E). The BMs were counterstained with an anti–laminin-γ1 chain antibody (magenta). The open and closed arrowheads indicate the mesonephric duct and ureteric bud, respectively. The asterisks indicate nonspecific binding of the anti-QBRICK antibody to the mesenchyme. Bars, 50 µm. (F) The expression levels of *Gdnf* and *Pax2* transcripts in the E11.5 metanephros of *Qbrick*$^{+/-}$ control (open bars) and *Qbrick*$^{-/-}$ (shaded bars) littermates were determined by quantitative RT-PCR and normalized by the expression level of *Gapdh*. The expression level in control mice was set at 1. Each bar represents the mean ± SD (error bars; $n = 3$). **, $P < 0.01$, significant difference by Student's *t* test.

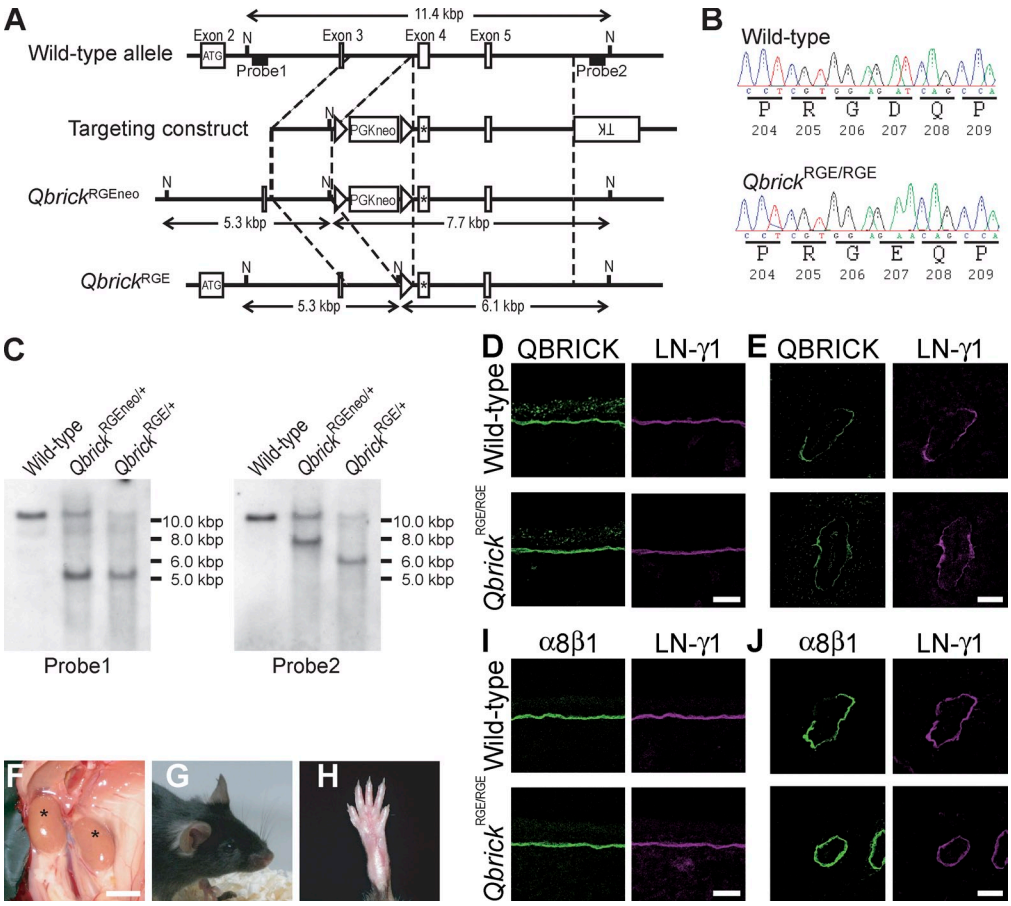

Figure 3. **Generation of *Qbrick*$^{RGE/RGE}$ mice.** (A) Schematic representation of the targeted mutation of *Qbrick*. Open boxes represent exons. The knock-in construct was designed to replace exon 4, which contains the codon encoding Asp207, with a mutated exon (open box with asterisk) in which the codon encoding Asp207 was substituted with a codon encoding Glu207. The probes used for Southern blotting are indicated by bold lines. N, NcoI restriction site; TK, thymidine kinase. (B) Direct DNA sequencing of the wild-type and *Qbrick*$^{RGE/RGE}$ genomes. The numbers indicate the positions of the amino acids in the primary sequence of QBRICK protein. (C) Southern blot analyses of genomic DNA from wild-type, *Qbrick*$^{RGEneo/+}$, and *Qbrick*$^{RGE/+}$ offspring after digestion with NcoI. Fragments of 5.3 and 7.7 kbp are detected with probe 1 and probe 2, respectively, indicating that the expected homologous recombination occurred. The detection of a 6.1-kbp fragment with probe 2 indicates that the neomycin resistance gene has been removed from the *Qbrick*^{RGEneo} allele by the Cre-loxP system. (D and E) Immunofluorescence staining (green) for QBRICK in E15.5 dorsal skin (D) and E11.5 ureteric buds (E). The BMs were counterstained with an anti–laminin-γ1 chain antibody (magenta). (F–H) *Qbrick*$^{RGE/RGE}$ mice develop normally without any defects in the kidneys (asterisks in F), eyelids (G), and digits (H). (I and J) Binding of recombinant integrin α8β1 (green) to E15.5 dorsal skin (I) and E11.5 ureteric buds (J). The BMs were counterstained with an anti–laminin-γ1 chain antibody (magenta). In panels D, E, I, and J, the top and bottom panels show fluorescence images for wild-type and *Qbrick*$^{RGE/RGE}$ littermates, respectively. The expression levels of QBRICK are comparable between wild-type and *Qbrick*$^{RGE/RGE}$ littermates. It should be noted that the binding of integrin α8β1 to the epidermal BMs of the E15.5 dorsal skin (I) as well as the E11.5 ureteric buds (J) is comparable between wild-type and *Qbrick*$^{RGE/RGE}$ littermates. Bars: (D and I) 20 µm; (E and J) 50 µm; (F) 5 mm.

diminished in the metanephros at E11.5 (Fig. 2 F), the stage when *Gdnf* reduction is observed in integrin α8–deficient mice (Linton et al., 2007). The expression of *Pax2*, a transcription factor critical for metanephric development, remained unaffected in the *Qbrick*$^{-/-}$ metanephros (Fig. 2 F), similar to the case for integrin α8–deficient mice (Linton et al., 2007). These findings are consistent with the view that the loss of QBRICK impairs integrin α8β1–mediated signaling, which eventually results in renal dysgenesis.

The RGD-dependent integrin-binding activity of QBRICK is dispensable for BMs to interact with integrin α8β1

Next, we investigated whether the diminished integrin α8β1 binding in *Qbrick*$^{-/-}$ embryos could be a direct consequence of the absence of the integrin binding ability of QBRICK. To address this possibility, we generated knock-in animals, *Qbrick*^{RGE} mice, in which the RGD integrin-binding motif in QBRICK was substituted with Arg-Gly-Glu (RGE) to inactivate the integrin α8β1 binding activity (Fig. 3, A–C). Immunofluorescence staining showed that *Qbrick*$^{RGE/RGE}$ mice expressed the mutant QBRICK^{RGE} protein at comparable levels to those of QBRICK in wild-type mice at the BMs of the embryonic skin (Fig. 3 D), ureteric bud (Fig. 3 E), lung, and choroid plexus (Fig. S1, A and B). The expression levels of Fras1 and Frem2 also remained unaltered in *Qbrick*$^{RGE/RGE}$ embryos (Fig. S1, C–H). *Qbrick*$^{RGE/RGE}$ mice were born at the expected Mendelian ratios (wild-type/heterozygous/homozygous = 34:80:36) and phenocopied neither the renal defects observed in integrin α8–null mice and FS model mice (Fig. 3 F) nor the other developmental defects associated with FS, namely cryptophthalmos, syndactyly, and dystrophic epidermolysis bullosa (Fig. 3, G and H;

and not depicted). Furthermore, the integrin α8β1 binding to the BMs of the epidermis (Fig. 3 I), ureteric bud (Fig. 3 J), lung, and choroid plexus (Fig. S1, I and J) appeared unaffected in *Qbrick*$^{RGE/RGE}$ embryos, indicating that QBRICK accounts for only a small fraction of the ability of BMs to bind integrin α8β1. These findings indicate that QBRICK regulates integrin α8β1 binding and renal development independently of its own integrin-binding activity.

QBRICK regulates the expression of the other integrin α8β1 ligands nephronectin and MAEG

Given the impaired BM binding of integrin α8β1 in *Qbrick*$^{-/-}$ mice, we examined the alternative possibility that QBRICK regulates the expression of other integrin α8β1 ligands in BMs. We focused on nephronectin and its homologue MAEG, both of which are localized at BMs and serve as ligands for integrin α8β1 (Brandenberger et al., 2001; Osada et al., 2005). In *Qbrick*$^{-/-}$ littermates, nephronectin was detected at the epidermal BM, but its immunoreactivity was greatly diminished compared with wild-type littermates (Fig. 4 A). Similarly, the expression of MAEG was reduced in the *Qbrick*$^{-/-}$ epidermal BM (Fig. 4 B). Diminished expression of nephronectin and MAEG was also apparent in the BMs of the developing lungs and choroid plexus in *Qbrick*$^{-/-}$ embryos (Fig. S2). Reduced expression of nephronectin and MAEG at embryonic BMs was also observed in other FS animal models, i.e., *Frem2*$^{my/my}$ and *Grip1*$^{eb/eb}$ mice (Fig. 4, C–F), where the BM deposition of QBRICK was greatly diminished (Fig. 1).

Nephronectin has been shown to play a critical role in renal development (Linton et al., 2007). In the developing kidney, nephronectin was detected at the BM of the mesonephric duct at E10.5 and that of the ureteric bud at E11.5 (Fig. 4, G and H), which is consistent with a previous study (Brandenberger et al., 2001). MAEG was undetectable at these renal BMs (Fig. 4, I and J). In *Qbrick*$^{-/-}$ embryos, the expression of nephronectin was greatly diminished at the BMs of the developing metanephros (Fig. 4, G and H), which is consistent with its scarce expression in the BMs of the epidermis and other organs. The diminished expression of nephronectin and MAEG in *Qbrick*$^{-/-}$ mice was further confirmed by Western blot analyses of tissue extracts from embryonic kidneys and skin (Fig. 4, K–M). No differences in the expression levels of laminin and integrin α8 were detected between wild-type and *Qbrick*$^{-/-}$ mice by the same analyses. Similar results were obtained when tissue extracts from *Frem2*$^{my/my}$ and *Grip1*$^{eb/eb}$ embryos were analyzed by Western blotting (Fig. 4, N and O). In contrast, diminished expression of nephronectin and MAEG was not observed in *Qbrick*$^{RGE/RGE}$ embryos (Fig. S3), indicating that the BM assembly of nephronectin and MAEG is independent of the ability of QBRICK to interact with integrin α8β1.

Although QBRICK and MAEG have been shown to possess an RGD motif and mediate integrin α8β1–dependent cell adhesion (Kiyozumi et al., 2005; Osada et al., 2005), their direct interactions with integrin α8β1 have not been demonstrated. Solid-phase binding assays using recombinant integrin α8β1 demonstrated that QBRICK and MAEG were capable of binding to integrin α8β1 with only weak affinities that were more than two orders of magnitude less than that of nephronectin (Fig. 4 P). These results indicate that nephronectin is the major determinant for the ability of BMs to bind integrin α8β1, which is consistent with the observation that the ability of BMs to bind integrin α8β1 remained uncompromised in *Qbrick*$^{RGE/RGE}$ embryos. These findings raise the possibility that QBRICK defines the ability of BMs to interact with integrin α8β1 by regulating the assembly of nephronectin, a high-affinity ligand for integrin α8β1, into BMs.

Integrin α8β1 binding by MAEG is dispensable for embryonic development

The weak binding of MAEG to integrin α8β1 makes it unlikely that the decreased integrin α8β1 binding to the BMs of *Qbrick*$^{-/-}$ mice is caused by reduced expression of MAEG. To further exclude this possibility, we generated mutant mice in which the RGD motif was deleted from MAEG. Because the RGD sequence of MAEG is located within a central linker segment, we generated mutant mice in which exons 9 and 10 of the *Maeg* gene encoding the linker segment were deleted (Fig. 5, A–D). The resulting mutant mice (*Maeg*$^{\Delta RGD}$) were apparently normal and did not phenocopy any FS-like developmental defects (unpublished data). In *Maeg*$^{\Delta RGD}$ mice, the mutant MAEG protein was still localized at the embryonic epidermal BM (Fig. 5, E and F). The expression levels of QBRICK and nephronectin at the epidermal BMs were comparable between wild-type and *Maeg*$^{\Delta RGD}$ embryos at E15.5 (Fig. 5, G and H). Western blotting analyses further showed that the expression levels of nephronectin and integrin α8 in the embryonic skin and kidney were comparable between *Maeg*$^{\Delta RGD}$ and wild-type littermates (Fig. 5, I and J). The binding of integrin α8β1 was also comparable between the mutant mice and wild-type littermates (Fig. 5 K), which indicates that the contribution of MAEG to the integrin α8β1 binding activity of BMs is only marginal.

FS-associated BM proteins are capable of binding to nephronectin and MAEG

Given the reduced BM deposition of nephronectin and MAEG in *Qbrick*$^{-/-}$ mice, we sought to further clarify how QBRICK modulates the assembly of nephronectin and MAEG into BMs. The levels of *Npnt* as well as *Maeg* transcripts in the E15.5 skin and whole embryos remained unaffected in *Qbrick*$^{-/-}$ mice (Fig. 6, A and B), indicating that QBRICK regulates the assembly of nephronectin and MAEG into BMs at a posttranscriptional level. Immunofluorescence examination of the embryonic skin at high-power magnification did not reveal any abnormal intracellular deposition of nephronectin or MAEG inside the epithelial and mesenchymal cells that faced each other across a BM (Fig. 6 C), making it unlikely that the secretion of nephronectin and MAEG was impaired by QBRICK deficiency. Furthermore, the expression levels of 18 different BM components were unaffected in *Qbrick*$^{-/-}$ embryos (Fig. S4). These findings indicate that the diminished assembly of nephronectin and MAEG occurs specifically and is not caused by a gross defect in the BM architecture.

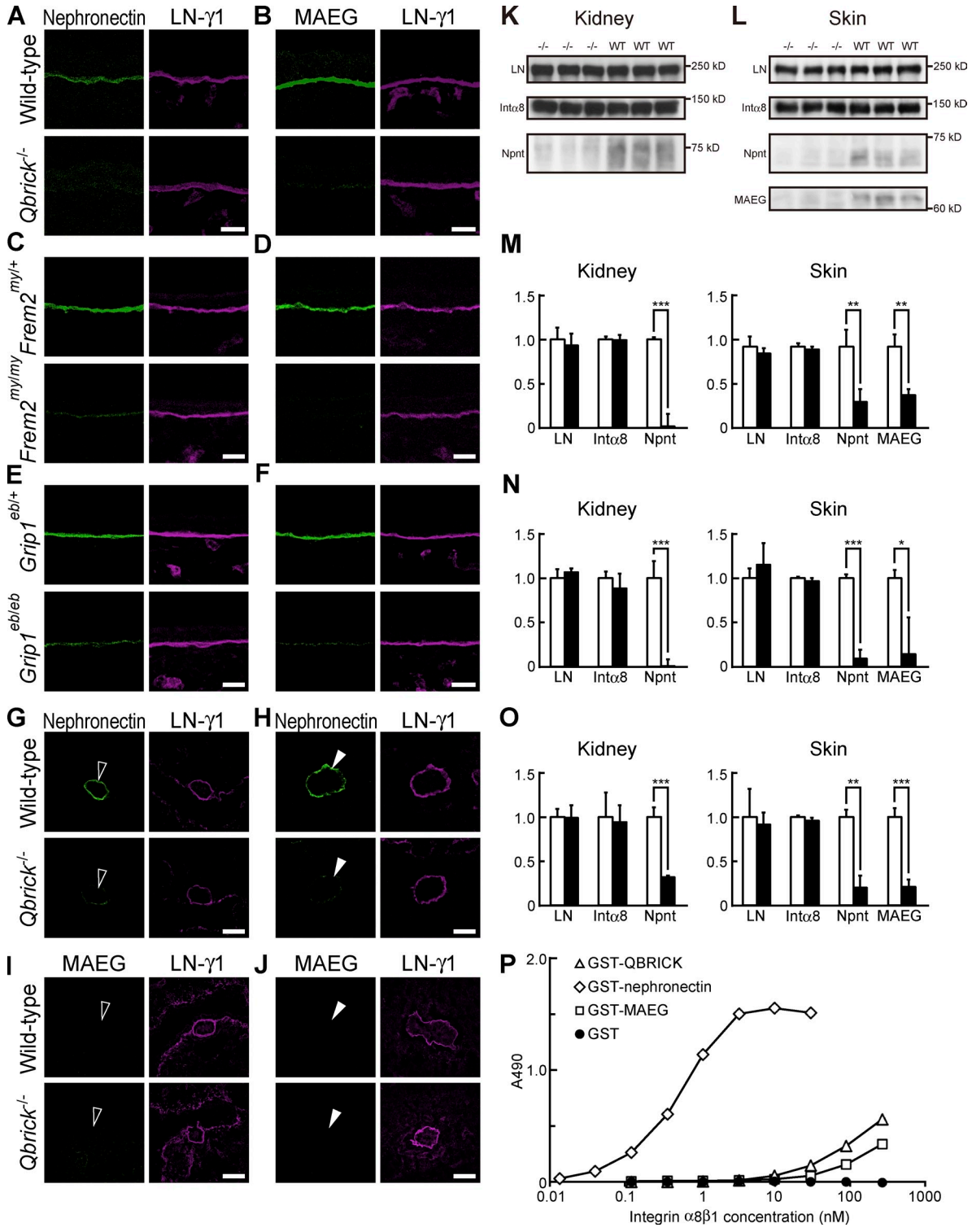

Figure 4. **Impaired expression of nephronectin and MAEG in FS model mice.** (A–F) Immunofluorescence staining (green) for nephronectin (A, C, and E) and MAEG (B, D, and F) in the dorsal skin of *Qbrick*$^{-/-}$ (A and B), *Frem2*$^{my/my}$ (C and D), and *Grip1*$^{eb/eb}$ (E and F) mice, and their control wild-type or heterozygous littermates. (G–J) Immunofluorescence staining (green) for nephronectin (G and H) and MAEG (I and J) at the E10.5 mesonephric duct (G and I; open arrowheads) and E11.5 ureteric bud (H and J; closed arrowheads) in wild-type (top) and *Qbrick*$^{-/-}$ (bottom) littermates. The BMs were counterstained with an anti–laminin-γ1 chain antibody (magenta). Bars: (A–F) 20 µm; (G–J) 50 µm. (K and L) Immunoblot detection of laminin β1 and γ1 chains (LN), integrin α8 (Intα8), nephronectin (Npnt), and MAEG in protein extracts from the kidney (K) and skin (L) of E15.5 *Qbrick*$^{-/-}$ mice and their wild-type littermates. (M–O) Immunoblot signal intensities of laminin, integrin α8, nephronectin, and MAEG in the kidney (left) and skin (right) of E15.5 wild-type (open bars) and *Qbrick*$^{-/-}$ (shaded bars; M), E15.5 *Frem2*$^{my/+}$ (open bars) and *Frem2*$^{my/my}$ (shaded bars; N), and E17.5 *Grip1*$^{eb/+}$ (open bars) and *Grip1*$^{eb/eb}$ (shaded bars; O) mice. The signal levels in control mice were set at 1. Each bar represents the mean ± SD (error bars; n = 3–6). *, P < 0.05; **, P < 0.01; ***, P < 0.001, significant differences by Student's t tests. (P) Titration curves of recombinant integrin α8β1 bound to the GST-fused NV domain of QBRICK (open triangles), GST-fused RGD linker segment of nephronectin (open diamonds), GST-fused RGD linker segment of MAEG (open squares), and GST (closed circles). Each point represents the mean ± SEM (n = 3).

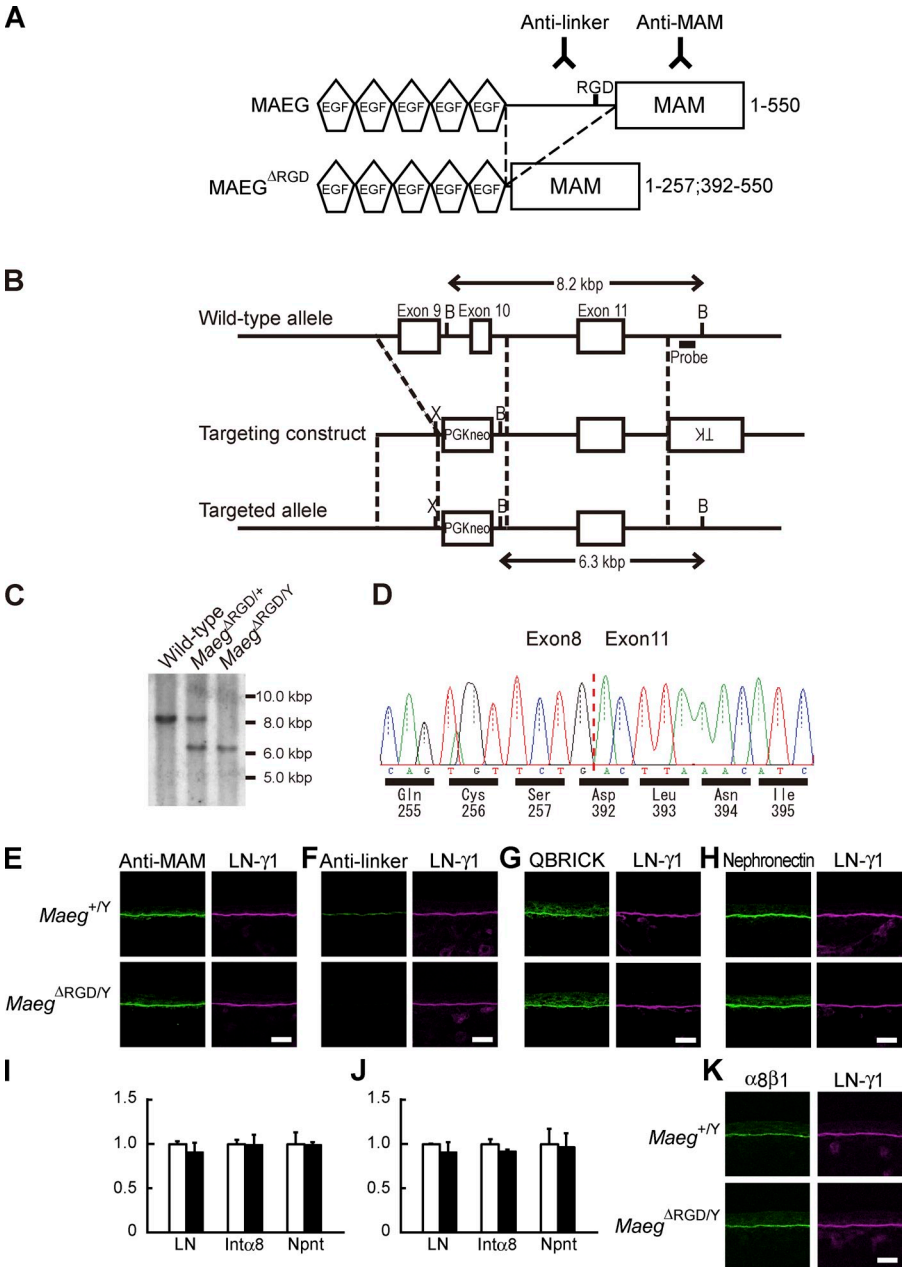

Figure 5. **The binding of integrin α8β1 to BMs is not compromised in *Maeg*$^{\Delta RGD}$ mice.** (A) Schematic views of MAEG and MAEG$^{\Delta RGD}$, a deletion mutant lacking the linker segment. The sites recognized by the anti-MAEG antibodies (Anti-linker and Anti-MAM) are also shown. (B) Schematic representation of the targeted mutation of *Maeg*. Open boxes represent exons. The targeting construct was designed to replace exons 9 and 10, which encode the linker region, with PGKneo. The probes used for Southern blotting are indicated by bold lines. B, BamHI restriction site; TK, thymidine kinase. (C) Southern blot analysis of genomic DNA from wild-type, *Maeg*$^{\Delta RGD/+}$, and *Maeg*$^{\Delta RGD/Y}$ mice digested with BamHI. The detection of a 6.3-kbp fragment instead of an 8.2-kbp fragment indicates the presence of the mutated allele. (D) Direct DNA sequencing of the *Maeg*$^{\Delta RGD/Y}$-derived RT-PCR product demonstrating that the open reading frame has not shifted. The product encodes a polypeptide lacking amino acids 258–391 of the 550–amino-acid full-length sequence. The boundary between exons 8 and 11 is shown by the red broken line. The numbers indicate the positions of the corresponding amino acids in the wild-type MAEG sequence. (E and F) In E15.5 dorsal skin epidermal BMs, MAEG is comparably detected by immunofluorescence (green) in both *Maeg*$^{+/Y}$ and *Maeg*$^{\Delta RGD/Y}$ littermates with the anti-MAM antibody (E), but is only detected in *Maeg*$^{+/Y}$ embryos by the anti-linker antibody (F). (G, H, and K) Immunofluorescence staining for QBRICK (G, green) and nephronectin (H, green), and binding of recombinant integrin α8β1 (K, green) to epidermal BMs of the E15.5 dorsal skin are comparable between *Maeg*$^{+/Y}$ and *Maeg*$^{\Delta RGD/Y}$ littermates. The BMs were counterstained with an anti–laminin-γ1 chain antibody (magenta). In each set of panels, the top and bottom panels show fluorescence images for wild-type *Maeg*$^{+/Y}$ and *Maeg*$^{\Delta RGD/Y}$ littermates, respectively. Bars, 20 μm. (I and J) Immunoblot signal intensities of laminin β1 and γ1 chains (LN), integrin α8 (Intα8), and nephronectin (Npnt) in the kidney (I) and skin (J) of E15.5 control *Maeg*$^{+/Y}$ (open bars) and *Maeg*$^{\Delta RGD/Y}$ (shaded bars) mice. The signal levels in control mice were set at 1. Each bar represents the mean ± SD (error bars; $n = 3$).

Next, we addressed the possibility that QBRICK and/or other FS-associated proteins, i.e., Fras1 and Frem2, associate with nephronectin and MAEG, thereby anchoring these proteins at BMs. When nephronectin was immunoprecipitated from embryonic kidney extracts, QBRICK and Frem2 were also pulled down (Fig. 6 D). To further corroborate the association of nephronectin with QBRICK and other FS-associated proteins, we coexpressed FLAG-tagged nephronectin with QBRICK, Fras1, or Frem2 in 293F cells, and immunoprecipitated nephronectin from conditioned media with an anti-FLAG antibody. QBRICK, Fras1, and Frem2 were coprecipitated with nephronectin, but not with albumin cotransfected instead of nephronectin as a negative control (Fig. 6 F). We also performed similar experiments using nephronectin deletion mutants (Fig. 6 E). Deletion of the MAM domain, but not the EGF domain, significantly reduced the coprecipitation of QBRICK, Fras1, and Frem2. The RGD-containing linker segment pulled down none of the FS-associated proteins, suggesting that the segment is dispensable for the interactions of nephronectin with FS-associated proteins. Similarly, QBRICK, Fras1, and Frem2 were coimmunoprecipitated with MAEG, despite the finding that the EGF domain, rather than the MAM domain, was involved in the coimmunoprecipitation (Fig. 6 G). Immunoelectron microscopic observations revealed that nephronectin was localized at the sublamina densa region of the epidermal BM (Fig. 6 H), which is the region just beneath the lamina densa where QBRICK, Fras1, and Frem2 are also localized (Kiyozumi et al., 2006; Dalezios et al., 2007; Petrou et al., 2007a,b), in E15.5 embryos. Collectively, these findings indicate that QBRICK, together with Fras1 and Frem2, interacts with nephronectin (and MAEG) at the sublamina densa region and thereby regulate the assembly of these integrin ligands into BMs.

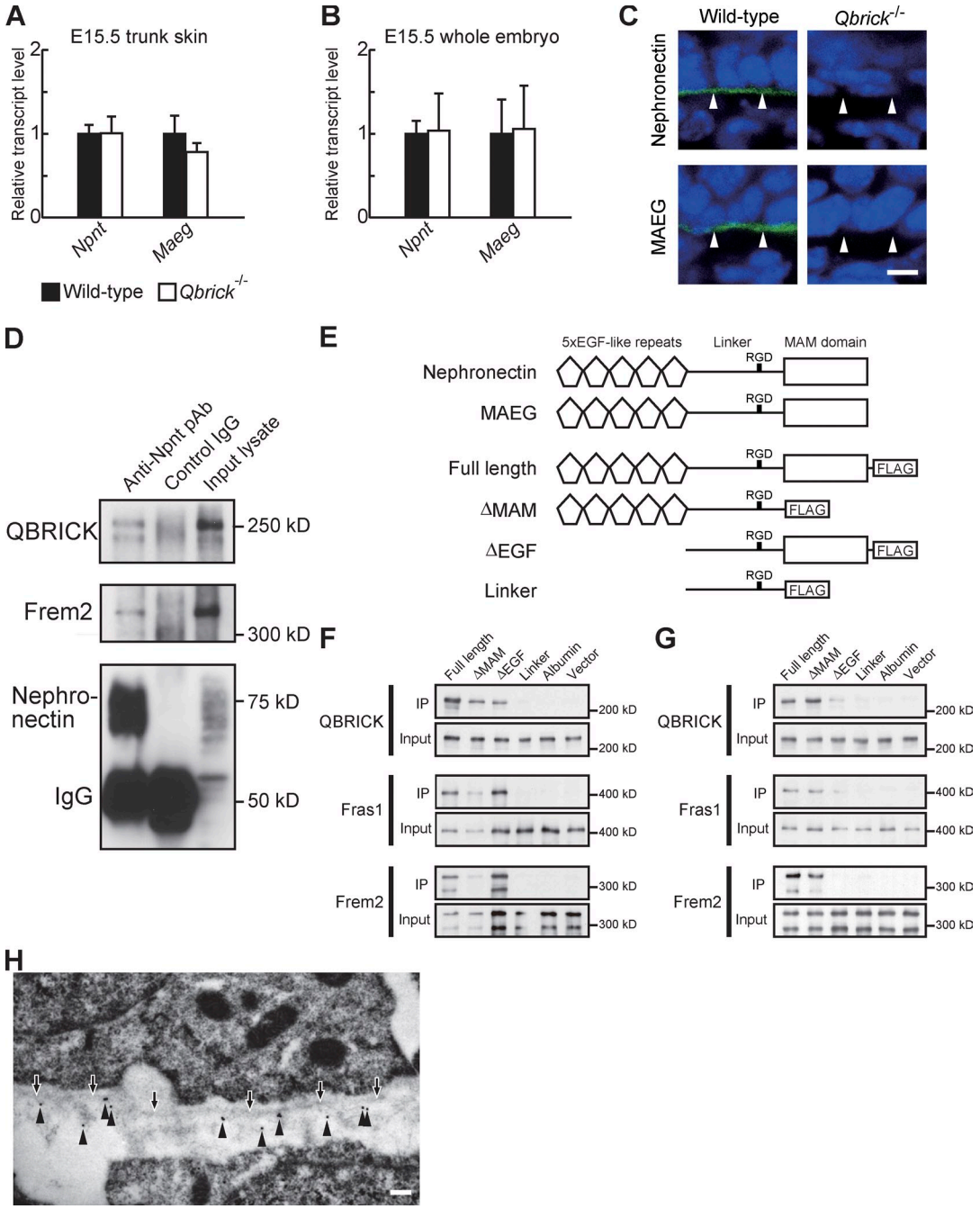

Figure 6. **Nephronectin and MAEG associate with QBRICK, Fras1, and Frem2 in vitro.** (A and B) The expression levels of *Npnt* and *Maeg* transcripts in E15.5 dorsal skin (A) and E15.5 whole embryos (B) of wild-type (shaded bars) and *Qbrick*$^{-/-}$ (open bars) littermates were determined by quantitative RT-PCR and normalized by the expression level of *Gapdh*. The expression level in wild-type mice was set at 1 for each transcript. Each bar represents the mean ± SD (in A, $n = 6$ for both wild-type and *Qbrick*$^{-/-}$; in B, $n = 5$ for wild-type and $n = 6$ for *Qbrick*$^{-/-}$). (C) Magnified views of epidermal basal cells (nephronectin producers) and dermal mesenchymal cells (MAEG producers) of E15.5 wild-type and *Qbrick*$^{-/-}$ mice stained with anti-nephronectin (top) and anti-MAEG (bottom) antibodies. The arrowheads indicate the position of the epidermal BMs. Bar, 5 µm. (D) E15.5 mouse kidney extracts were subjected to immunoprecipitation with an anti-nephronectin antibody or control rabbit IgG, and the resulting immunoprecipitates were analyzed by immunoblotting with anti-QBRICK, anti-Frem2, and anti-nephronectin antibodies. (E) Schematic views of FLAG-tagged nephronectin, MAEG, and their deletion mutants used for coimmunoprecipitation assays. (F) FLAG-tagged nephronectin or its deletion mutants were coexpressed with QBRICK, Fras1, or Frem2 and immunoprecipitated with an anti-FLAG monoclonal antibody. Proteins in the input samples or immunoprecipitates were specifically detected with anti-QBRICK, anti-HA (for Fras1), and anti-Myc (for Frem2) antibodies. (G) Coimmunoprecipitation experiments were performed for MAEG and its deletion mutants in a similar manner to those for nephronectin and its deletion mutants. (H) Immunoelectron microscopic analysis of embryonic skin. Ultrathin sections of ventral skin from E15.5 mouse embryos were labeled with an anti-nephronectin antibody, which was visualized by a 15-nm gold particle–conjugated secondary antibody. Nephronectin is located in the sublamina densa region of the epidermal BM (arrowheads). The arrows indicate the lamina densa. Bar, 200 nm.

Discussion

In the present study, we have demonstrated that the BMs of *Qbrick*$^{-/-}$ and other FS model animals show defects in binding to integrin α8β1, and that these defects arise from the diminished expression of nephronectin, but not QBRICK per se, at the BMs. Our data also showed that MAEG, another RGD-containing integrin α8β1 ligand, fails to stably assemble into BMs in these FS model animals, revealing a hitherto unknown mechanism that operates in the coordinated BM assembly of the three integrin α8β1 ligands, nephronectin, QBRICK, and MAEG. To the best of our knowledge, this is the first demonstration that QBRICK and other FS-associated BM proteins play a critical role in the BM assembly of integrin α8β1 ligands and thereby regulate the interactions of cells with BMs via integrin α8β1 and the signaling events thereafter.

Molecular mechanism of the BM assembly of nephronectin and MAEG

Because the expression levels of *Npnt* and *Maeg* transcripts remained unaffected in *Qbrick*$^{-/-}$ and other FS model mice, the diminished expression of nephronectin and MAEG at the BMs of these mutant mice probably results from defects in post-transcriptional events, namely impaired secretion or increased turnover of these proteins. Given that no intracellular inclusions of nephronectin and MAEG were detected in the epithelial and mesenchymal cells that faced each other across a BM in *Qbrick*$^{-/-}$ mice, the diminished BM deposition of these integrin α8β1 ligands does not seem to result from impaired secretion, but rather from increased turnover. Although the mechanisms for the turnover of nephronectin and MAEG in vivo remain to be elucidated, our data show that these RGD-containing integrin α8β1 ligands are associated with QBRICK and other FS-associated proteins in vivo, as indicated by the coimmunoprecipitation of nephronectin with QBRICK and Frem2 from embryonic tissue extracts. The interactions of nephronectin as well as MAEG with QBRICK and other FS-associated proteins were also confirmed by coimmunoprecipitation of these proteins after recombinant expression in 293-F cells in vitro. Thus, it seems likely that the three FS-associated proteins forming a ternary complex at the sublamina densa region serve as a scaffold for the stable association of nephronectin and MAEG with BMs via direct or indirect interactions with these α8β1 ligands. In support of this possibility, nephronectin was found to be localized at the sublamina densa region by immunoelectron microscopy. The failure of the association of nephronectin and MAEG with the ternary complex of FS-associated proteins may well render these α8β1 ligands more susceptible to proteolytic degradation and lead to their increased turnover at BMs in *Qbrick*$^{-/-}$ and other FS model animals, irrespective of the causative mutation.

Pathogenesis of the renal dysmorphogenesis in FS

Among the developmental defects observed in FS animals, the renal defects overlap with those observed in integrin α8–deficient mice. Initial outgrowth of the ureteric bud often fails or is delayed in both types of animals (Carter, 1959; Müller et al., 1997; McGregor et al., 2003; Pitera et al., 2008). To explain this phenotypic overlap, we obtained evidence that the integrin α8β1 binding by ureteric bud BMs was significantly impaired in the developing kidney of *Qbrick*$^{-/-}$ mice. The reduced integrin α8β1 binding in *Qbrick*$^{-/-}$ embryos was not caused by the lack of integrin α8β1 binding ability of QBRICK itself, but rather by the impaired expression of nephronectin, a high-affinity ligand for integrin α8β1. The expression of another ligand, MAEG, at BMs was also impaired in *Qbrick*$^{-/-}$ mice, but the contribution of MAEG as an integrin α8β1 ligand at BMs appears to be only marginal compared with that of nephronectin. Besides its weak activity for binding integrin α8β1, MAEG was hardly detected at the BM of the ureteric bud. Furthermore, *Maeg*$^{\Delta RGD}$ mice developed normally and did not exhibit renal defects, making it unlikely that MAEG is involved in the renal defects in *Qbrick*$^{-/-}$ mice. In contrast, nephronectin-deficient mice exhibit clear defects in renal morphogenesis (Linton et al., 2007). Direct integrin binding assays revealed that nephronectin has an exceptionally high affinity for integrin α8β1 with a subnanomolar dissociation constant (Sato et al., 2009; this paper), whereas QBRICK and MAEG have affinities for integrin α8β1 that are more than two orders of magnitude less than that of nephronectin, thus emphasizing the importance of nephronectin as a physiological ligand for integrin α8β1. We also found that reduced *Gdnf* expression, to which the renal phenotypes of integrin α8–deficient mice and nephronectin-deficient mice have been attributed (Linton et al., 2007), was recapitulated in the developing kidney of *Qbrick*$^{-/-}$ mice. Reduced *Gdnf* expression was also found in the metanephros of *Fras1* mutant mice (Pitera et al., 2008). Given that nephronectin functions as a dominant ligand for integrin α8β1 at the ureteric bud BM and plays a central role in renal morphogenesis via the induction of *Gdnf* expression, we propose a model for the pathogenesis of the renal defects in FS, as schematically illustrated in Fig. 7. In this model, aberrant expression of QBRICK or other FS-associated BM proteins destabilizes the ternary complex of FS-associated proteins and results in the loss of FS-associated proteins from the ureteric bud BM (Kiyozumi et al., 2006; this paper). The absence of FS-associated proteins leads to failure of nephronectin assembly at the sublamina densa region of the BM, and therefore metanephric mesenchymal cells expressing integrin α8β1 cannot interact with the ureteric bud BM to induce the signaling events necessary for the induction of *Gdnf* in metanephric mesenchymal cells. As a consequence, the expression of *Gdnf* is attenuated and renal developmental defects occur. Our results showed that the reduction in *Gdnf* expression was only partial (∼50%) in the *Qbrick*$^{-/-}$ metanephros. Nevertheless, this reduction may suffice to cause renal defects in *Qbrick*$^{-/-}$ mice, because renal agenesis sometimes occurs even in *Gdnf*$^{+/-}$ heterozygotes (Moore et al., 1996; Pichel et al., 1996; Sánchez et al., 1996).

It should be emphasized that >90% of *Qbrick*$^{-/-}$ mice exhibited either bilateral or unilateral renal agenesis. This is in striking contrast to the renal phenotype of another *Qbrick* mutant strain, called *bat* mice, in which only 20% of the mice

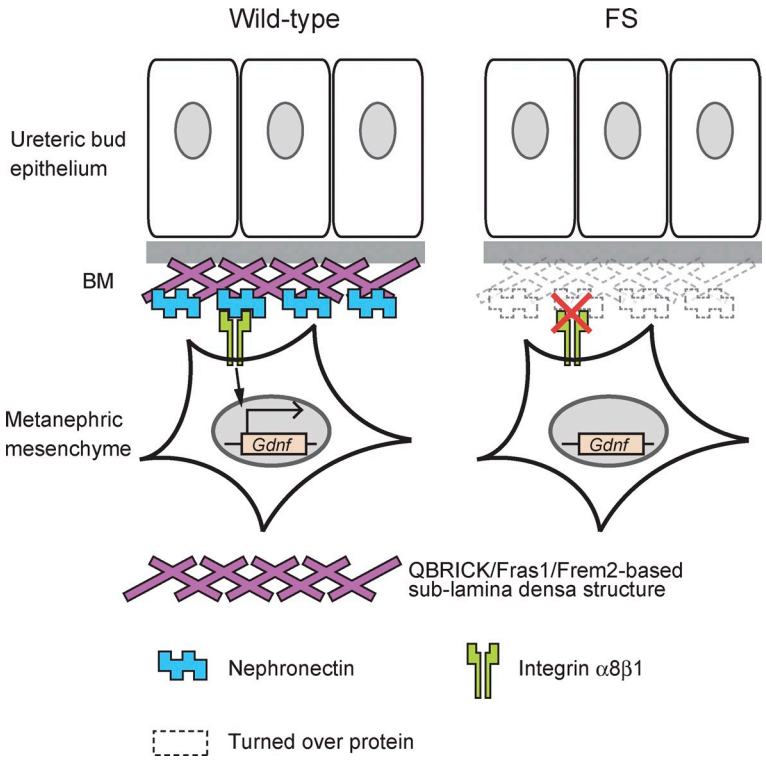

Figure 7. **A model for renal defects in FS.** In the developing metanephros, QBRICK and other FS-associated proteins associate with nephronectin in the sublamina densa region and secure its localization at BMs. Metanephric mesenchymal cells interact with nephronectin through integrin α8β1. Stimulation of integrin α8β1 induces *Gdnf*, which is necessary for further development of the metanephros (left). In FS, nephronectin is not stably deposited at BMs, owing to the loss of FS-associated proteins, and is eventually degraded. The loss of nephronectin leads to failure of *Gdnf* induction and subsequent metanephric development (right).

possess renal defects (Smyth et al., 2004). The apparent discrepancy between these two *Qbrick* mutant mice may result from the residual activity of QBRICK in *bat* mice, because the *Qbrick* transcripts from the *bat* allele encode a truncated QBRICK protein (Smyth et al., 2004). The resulting truncated protein may partially retain the ability to form a ternary complex with Fras1 and Frem2, and thereby cause only a partial defect in the stable localization of nephronectin at renal BMs. However, it remains to be determined whether the truncated QBRICK protein as well as nephronectin can be detected at the ureteric bud BM in *bat* mice.

Physiological roles of nephronectin and MAEG at BMs

Among the developmental defects observed in FS, dystrophic epidermolysis bullosa, syndactyly, and cryptophthalmos arise from defects in dermal–epidermal interactions. Both nephronectin and MAEG are highly expressed at the epidermal BM, implying their physiological roles in dermal–epidermal interactions. Because the dermal–epidermal integrity appears unaffected in mice deficient in integrin α8 (Müller et al., 1997), their functions as integrin α8β1 ligands seem to be dispensable for dermal–epidermal interactions. Besides their roles as integrin α8β1 ligands, they may function as linker components that anchor the epidermal BM to the mesenchymal ECM via associations with QBRICK, Fras1, and Frem2. Recently, nephronectin and MAEG were shown to function as BM components that anchor the arrector pili muscle to the BMs at the bulge of hair follicles (Fujiwara et al., 2011). These findings support the possibility that nephronectin and MAEG function as attachment sites that physically connect epidermal BMs with mesenchymal cells and/or ECMs. Apparently, nephronectin-null mice do not exhibit dystrophic epidermolysis bullosa, syndactyly, or cryptophthalmos (Linton et al., 2007). Because nephronectin and MAEG share the ability to associate with QBRICK, Fras1, and Frem2, it seems possible that MAEG compensates for the loss of nephronectin as a linker component, as has been shown for the attachment of the arrector pili muscle to the bulge BMs. It will therefore be interesting to examine whether ablation of both *Npnt* and *Maeg* recapitulates the defective dermal–epidermal interactions observed in FS model animals. It will also be interesting to investigate whether there are extracellular factors other than nephronectin and MAEG that can associate with FS-associated BM proteins. One such candidate is hemicentin-1, an ECM molecule critical for dermal–epidermal integrity in zebrafish (Carney et al., 2010). The hemicentin-1 nonsense mutation *nagel* was shown to cause epidermal blistering in a synergistic manner with the Fras1 mutation *pinfin* (Carney et al., 2010).

Possible role of the FS-associated proteins in epithelial–mesenchymal interactions

The stable expression of the three FS-associated proteins is strongly dependent on the concerted expression of all three proteins. QBRICK is secreted by mesenchymal cells, whereas Fras1 and Frem2 are secreted by epithelial cells. Thus, the BM assembly of these proteins requires appropriate cooperation of the epithelium and mesenchyme. Furthermore, the degree of the reciprocal stabilization of these proteins reflects how the interacting epithelium and mesenchyme fit with one another. Our data show that the expression of nephronectin and MAEG is regulated by the integrity of the three FS-associated BM proteins, and is therefore dependent on the combination between the epithelium and mesenchyme. Such regulated expression of

RGD-containing integrin ligands at BMs should be important for their function as signal transducers in epithelial–mesenchymal interactions because their expression needs to be fine-tuned spatially and temporally as organs develop. Nephronectin, which is expressed in the ureteric bud epithelium and recognized by integrin α8β1 expressed on the surface of the metanephric mesenchyme, is a typical "epithelium-to-mesenchyme" signal transducer. Regulated BM assembly of nephronectin by the FS-associated proteins would therefore facilitate the spatiotemporally regulated crosstalk between the epithelium and mesenchyme during renal development.

In summary, we have presented evidence that QBRICK, together with Fras1 and Frem2, defines the ability of BMs to bind integrin α8β1 through modulating the BM assembly of nephronectin, thereby regulating the integrin α8β1–mediated signals transmitted from the ureteric buds to the metanephric mesenchyme. Further investigations of these FS-associated BM proteins should provide insights into the pathogenesis of FS as well as the molecular basis of epithelial–mesenchymal interactions during development.

Materials and methods

Animals

Qbrick$^{-/-}$ mice were produced by a homologous recombination that substituted the second exon of the *Qbrick* gene, which includes an initiation codon, with a neomycin-resistance gene as described previously (Kiyozumi et al., 2006), and maintained in a C57BL/6 background. The *Frem2*^{my} MY/HuLeJ and *Grip1*^{eb} ATEB/LeJ mouse strains were obtained from Jackson ImmunoResearch Laboratories, Inc. Male MY/HuLeJ mice were outbred with female C57BL/6 mice, and the resulting *Frem2*$^{my/+}$ females were backcrossed to MY/HuLeJ males to obtain *Frem2*$^{my/my}$ and *Frem2*$^{my/+}$ littermates. Male ATEB/LeJ mice were outbred with female C57BL/6 mice, and the resulting *Grip1*$^{eb/+}$ females were backcrossed to ATEB/LeJ males to obtain *Grip1*$^{eb/eb}$ males. *Grip1*$^{eb/+}$ females and *Grip1*$^{eb/eb}$ males were crossed to obtain *Grip1*$^{eb/eb}$ and *Grip1*$^{eb/+}$ littermates, which were used for histological analyses. The B6.Cg-Tg(CAG-cre)CZ-MO2Osb mouse strain expressing Cre recombinase under the control of the CAG promoter (BRC No. 01828) was provided by Institute of Physical and Chemical Research (RIKEN) BioResource Center with the support of the National BioResource Project of the Ministry of Education, Culture, Sports, Science, and Technology, Japan.

To generate *Qbrick*^{RGE} knock-in mice, a knock-in vector was constructed as follows: the vector included the 2-kb upstream *Qbrick* genomic sequence, a neomycin resistance gene sandwiched by loxP sequences, the 5-kb downstream *Qbrick* genomic sequence, and a thymidine kinase gene (Fig. 3 A). To introduce the RGE mutation, the 5-kb genomic sequence was point-mutated by overlap extension PCR. The knock-in vector was introduced into strain 129 mouse embryonic stem cells. The resulting targeted clones were verified by PCR and Southern blotting, and injected into C57BL/6 blastocysts to obtain chimeric mice. The resulting male chimeric mice that transmitted the mutated *Qbrick* gene through the germline were crossed with C57BL/6 female mice to generate *Qbrick*$^{RGE(Neo)}$ mice. The resulting *Qbrick*$^{RGE(Neo)/+}$ heterozygotes were crossed with B6.Cg-Tg(CAG-cre)CZ-MO2Osb mice to obtain *Qbrick*$^{RGE/+}$ heterozygotes in which the neomycin resistance gene was removed. *Qbrick*$^{RGE/+}$ heterozygotes were maintained in a C57BL/6 background and crossed to obtain *Qbrick*$^{RGE/RGE}$ homozygotes and wild-type littermates.

To generate *Maeg*$^{\Delta RGD}$ mutant mice, we created a targeting construct in which the 2.0-kb upstream and 4.2-kb downstream *Maeg* genomic sequences flanked a neomycin resistance gene (Fig. 5 B). To substitute exons 9 and 10, which encode the linker region including the RGD sequence, with a neomycin resistance gene, the targeting vector was introduced into strain 129 mouse embryonic stem cells. The targeted clones were identified by PCR and Southern blotting, and injected into C57BL/6 blastocysts. The resulting chimeric male offspring that transmitted the mutated *Maeg* gene through the germline were crossed with C57BL/6 female mice to obtain *Maeg*$^{\Delta RGD/Y}$ male and *Maeg*$^{\Delta RGD/+}$ female mice. *Maeg*$^{\Delta RGD/Y}$ male and *Maeg*$^{\Delta RGD/+}$ female mice were maintained in a C57BL/6 background and crossed to obtain embryos lacking wild-type MAEG (*Maeg*$^{\Delta RGD/Y}$) and their control (*Maeg*$^{+/Y}$) littermates. All the mouse experiments were performed in compliance with the institutional guidelines and were approved by the Animal Care Committee of Osaka University.

Immunofluorescence

Embryos or newborn mice were embedded in OCT for cryosectioning. 10-µm sections were fixed in absolute ethanol for 20 min at –20°C, then rehydrated with PBS. The antibodies used and their concentrations are shown in Table S1. After incubation with primary antibodies at 4°C overnight, the sections were incubated with 1:3,000-diluted Alexa Fluor 488–conjugated goat anti–rabbit IgG (Invitrogen) and 1:4,000-diluted Cy3-conjugated anti–rat IgG (Jackson ImmunoResearch Laboratories) as secondary antibodies at 4°C for 2 h. To detect intracellular protein inclusions, frozen sections were fixed with 4% paraformaldehyde in PBS at 4°C for 15 min and permeabilized with 0.1% Triton X-100 in PBS at 4°C for 10 min before incubation with primary antibodies. The sections were mounted in Perma-Fluor (Thermo Fisher Scientific) and visualized using a laser scanning microscope (LSM5 PASCAL; Carl Zeiss) equipped with LD-Achroplan (20×, NA 0.4) and Plan-Neofluar (10×, NA 0.3; 40×, NA 0.75; 63×, NA 1.25) objective lenses at room temperature. The imaging medium was air for the 10×, 20×, and 40× objective lenses, and Immersol 518 F (Carl Zeiss) for the 63× objective lens. The LSM5 PASCAL software (Carl Zeiss) was used during image collection. Each set of stained sections was processed under identical gain and laser power settings. Each set of obtained images was processed under identical brightness and contrast settings, which were adjusted by the LSM image browser (Carl Zeiss) for clear visualization of BMs. At least four pairs of sections of mutant mice and their control littermates were examined, and similar results were obtained.

Immunoelectron microscopy

E15.5 mouse embryos were sequentially fixed in 0.5% glutaraldehyde and 4% paraformaldehyde in 30 mM Hepes, pH 7.4, 100 mM NaCl, and 2 mM $CaCl_2$. After dehydration, the samples were embedded in LR white resin. Ultrathin sections (70 nm) were labeled with a rabbit anti-nephronectin polyclonal antibody (Manabe et al., 2008), which was visualized using 15-nm gold particle-conjugated anti–rabbit IgG. The sections were post-stained with uranyl acetate and lead citrate. Images were acquired using a 1200EX electron microscope (JEOL Ltd.) operated at 80 kV.

Construction of plasmids for recombinant protein expression

A cDNA encoding the Ig κ-chain signal sequence followed by three tandem HA epitope tag sequences and Fras1 (amino acids 26–4,010) or a cDNA encoding the Ig κ-chain signal sequence followed by three tandem Myc epitope tag sequences and Frem2 (amino acids 40–3160) were cloned into pcDNA3.1(+) (Invitrogen) for expression of 3× HA-tagged Fras1 or 3× Myc-tagged Frem2, respectively, as described previously (Kiyozumi et al., 2006). A full-length QBRICK cDNA was subcloned into pcDNA3.1(+). A cDNA encoding full-length mouse albumin was cloned into pFLAG-CMV-5a (Sigma-Aldrich) for expression of FLAG-tagged albumin. A cDNA encoding full-length nephronectin was subcloned into pFLAG-CMV (Invitrogen) for expression of FLAG-tagged nephronectin, as described previously (Sato et al., 2009). For expression of nephronectin deletion mutant proteins, cDNAs encoding ΔEGF (amino acids 1–23:257–561), ΔMAM (amino acids 1–419), or the linker segment alone (amino acids 1–23:257–414) were individually subcloned into pFLAG-CMV, as described previously (Sato et al., 2009). Mouse MAEG cDNAs encoding amino acids 19–550 (full length), 19–393 (ΔMAM), 254–550 (ΔEGF), and 254–393 (linker) were amplified by PCR with the following primer pairs: full length, 5′-GGGGGCGCGCCGGAGTAGGGACCA-3′ and 5′-GGCCAGATCTACCTTCTACAGATAAAAAGT-3′; ΔMAM, 5′-GGGGGCGCGCCGGAGTAGGGACCA-3′ and 5′-CTGAAGATCTTAAGTCTTTGTGCTTCAGT-3′; ΔEGF, 5′-CTGCGGCGCGCCGTGATCCCTGAACATTC-3′ and 5′-GGCCAGATCTACCTTCTACAGATAAAAAGT-3′; and linker, 5′-CTGCGGCGCGCCGTGATCCCTGAACATTC-3′ and 5′-CTGAAGATCTTAAGTCTTTGTGCTTCAGT-3′. The cDNA fragments were subcloned into pSecFLAG, a modified vector of pSecTag2A (Invitrogen). The pSecFLAG vector was generated by subcloning a double-stranded DNA encoding the FLAG sequence followed by a stop codon (sense strand sequence: 5′-GGATCCGGTACCGATTACAAGGACGACGATGACAAGTAGCTCGAG-3′) using the BamHI and XhoI sites. The cDNA fragments were digested with AscI and BglII and subcloned into the pSecFLAG expression vector using the AscI and BamHI restriction sites. The resulting plasmids each contained an open reading frame expressing a polypeptide consisting of an N-terminal signal sequence, a MAEG protein fragment, and a C-terminal FLAG tag.

Plasmids expressing the human integrin α3, α6, α7X2, and α8 extracellular domains fused to the ACID peptide with a FLAG tag, and the β1 and β4 extracellular domains fused to the BASE peptide with a 5× His tag were prepared as previously described (Nishiuchi et al., 2006; Ido et al., 2007; Sato et al., 2009). cDNAs encoding an NV domain of QBRICK (amino acids 23–280), a linker segment of nephronectin (amino acids 256–414), or a linker segment of MAEG (amino acids 260–392) were individually subcloned into pGEX 4T-1 (GE Healthcare), as described previously (Kiyozumi et al., 2005; Osada et al., 2005; Sato et al., 2009).

Protein expression and purification

The recombinant integrins were expressed and purified as described previously (Nishiuchi et al., 2006). In brief, expression plasmids for a pair of integrin α and β subunits were cotransfected into 293-F cells (Invitrogen), and the recombinant integrins were purified from the conditioned medium using Ni-NTA affinity columns, followed by anti-FLAG mAb affinity chromatography.

Recombinant GST fusion proteins were induced in *Escherichia coli* by overnight incubation with 0.1 mM IPTG at 25°C. The cells were then lysed by sonication, and the supernatants were passed through a glutathione–Sepharose 4B column (GE Healthcare). The bound proteins were eluted with 50 mM Tris-HCl, pH 8.0, containing 10 mM glutathione.

In situ integrin binding

Frozen sections of mouse embryos were blocked with blocking buffer (3% BSA, 25 mM Tris-HCl, pH 7.4, 100 mM NaCl, and 1 mM $MnCl_2$) for 30 min at room temperature, then incubated with 1–10 µg/ml of recombinant integrins and a rat anti–laminin-γ1 monoclonal antibody (Millipore) in blocking buffer at 4°C overnight. After three washes with wash buffer (25 mM Tris-HCl, pH 7.4, 100 mM NaCl, and 1 mM $MnCl_2$) for 10 min at room temperature, the sections were incubated with 0.5 µg/ml of rabbit anti-Velcro (ACID/BASE coiled-coil) antibody (Takagi et al., 2001) in blocking buffer at room temperature for 2 h. The sections were then washed with wash buffer and incubated with 1:3,000-diluted Alexa Fluor 488–conjugated goat anti–rabbit IgG (Invitrogen) and 1:4,000-diluted Cy3-conjugated anti–rat IgG (Jackson ImmunoResearch Laboratories). After washing with wash buffer, the sections were mounted in PermaFluor (Thermo Fisher Scientific). The fluorescent probes were visualized with an LSM5 laser scanning microscope, as described for the immunofluorescence. At least four pairs of sections of mutant mice and their control littermates were examined, and similar results were obtained.

Solid-phase integrin binding assay

Solid-phase integrin binding assays were performed as described previously (Nishiuchi et al., 2006). In brief, microtiter plates were coated with substrate recombinant proteins (10 nM) overnight at 4°C, and then blocked with 1% BSA. The plates were incubated with recombinant integrin α8β1 in the presence of 1 mM $MnCl_2$. The plates were washed with TBS containing 1 mM $MnCl_2$, 0.1% BSA, and 0.02% Tween 20, followed by quantification of bound integrin α8β1 by ELISA using a biotinylated rabbit anti-Velcro antibody and HRP-conjugated streptavidin.

Quantitative RT-PCR

Quantitative RT-PCR was performed as described previously (Kiyozumi et al., 2006). The primers used were as follows: *Npnt*, 5′-TGAGGAAACACGGTACCCACGGAGC-3′ and 5′-AGGGGTCTTCTCAGCAGCGACCTCT-3′; *Maeg*, 5′-ATGAGGATGGAAGGTGGAGGACAGG-3′ and 5′-AGTCATCGGGACACAAGCCTGACAC-3′; *Gdnf*, 5′-GCTTCTCGAAGCGCCCGCTGAAGACCACT-3′ and 5′-CTTTTCAGTCTTTTAATGGTGGCTTGAATA-3′; *Pax2*, 5′-GATATGACGAGCACCACTCTACCTGGTTAC-3′ and 5′-ATTGTAGGCGGTGTACTGGGGATGGCTGTA-3′; and *Gapdh*, 5′-AATGGTGAAGGTCGGTGTG-3′ and 5′-TGGTGAAGACACCAGTAGA-3′. The expression levels of the individual transcripts were normalized by the expression level of *Gapdh*.

Western blotting

E15.5–E17.5 skin and kidneys were homogenized with SDS-PAGE sample buffer (2% SDS, 5% sucrose, and 63 mM Tris-HCl, pH 6.8), and the protein concentrations of the homogenates were determined using a BCA protein assay reagent kit (Thermo Fisher Scientific). The homogenates were supplemented with a 1/20 volume of 2-mercaptoethanol, boiled, and subjected to SDS-PAGE. The separated proteins were electrotransferred to a nitrocellulose membrane. The primary antibodies used were: rabbit anti-laminin (L9393; Sigma-Aldrich), goat anti–mouse integrin α8 (R&D Systems), rabbit anti-nephronectin (Manabe et al., 2008), and rabbit anti-MAEG (Osada et al., 2005). The bound primary antibodies were visualized with an Amersham ECL Prime Western blotting detection reagent kit (GE Healthcare). The intensities of the signals were quantified using ImageJ software (Abramoff et al., 2004).

Immunoprecipitation assays

Embryonic kidney extracts were prepared as described previously (Brandenberger et al., 2001), with slight modifications. In brief, E15.5 kidneys were homogenized in ice-cold TBS containing 1 mM PMSF, 0.7 µg/ml pepstatin A, and 10 µg/ml leupeptin using a Dounce homogenizer. After centrifugation at 18,000 *g* for 30 min, the pellet was resuspended in extraction buffer (20 mM Tris-HCl, pH 7.5, 150 mM NaCl, 1 mM $MgCl_2$, 1.5% *n*-octylglucoside, 1 mM PMSF, 0.7 µg/ml pepstatin A, and 10 µg/ml leupeptin), sonicated, and centrifuged at 10,000 *g* for 20 min to remove debris. An anti-nephronectin polyclonal antibody or rabbit IgG, which was immobilized on Protein A Sepharose 4 Fast Flow Beads (GE Healthcare), was added to the kidney extract and incubated for 6 h at 4°C with gentle rotation. The beads were washed with extraction buffer three times, followed by treatment with SDS-PAGE sample buffer. The supernatant was recovered by centrifugation and subjected to Western blotting analysis.

Immunoprecipitation was also performed using conditioned media containing recombinant proteins. Aliquots (5 ml) of Freestyle 293-F cells (Invitrogen) at 10^6 cells/ml were transfected with 4 µg of plasmids encoding 3× HA-tagged Fras1, 3× Myc-tagged Frem2, or QBRICK and 1 µg of plasmids encoding FLAG-tagged nephronectin, FLAG-tagged MAEG, or their deletion mutants using the 293Fectin transfection reagent (Invitrogen). After 3 d of culture, the conditioned media were recovered by centrifugation. The conditioned media were supplemented with a 1/20 volume of 1 M Tris-HCl, pH 7.4, a 1/10 volume of 10% Triton X-100, and a 1/38 volume of anti-FLAG M2 agarose beads (Sigma-Aldrich), and incubated at 4°C overnight with gentle rotation. The beads were washed three times with TBS containing 1 mM $CaCl_2$ and 1% Triton X-100. Proteins bound to the agarose beads were eluted with SDS-PAGE sample buffer and subjected to SDS-PAGE, followed by immunoblotting with anti-HA (Babco), anti-Myc (Santa Cruz Biotechnology, Inc.), anti-FLAG (Sigma-Aldrich), and anti-QBRICK (Kiyozumi et al., 2005) antibodies.

Online supplemental material

Fig. S1 shows the immunofluorescence and in situ integrin α8β1 binding of *Qbrick*$^{RGE/RGE}$ mice. Fig. S2 shows the immunofluorescence of nephronectin and MAEG in *Qbrick*$^{-/-}$ mice. Fig. S3 shows the immunofluorescence and immunoblotting analyses of nephronectin and MAEG in *Qbrick*$^{RGE/RGE}$ mice. Fig. S4 shows the immunofluorescence of various BM proteins in *Qbrick*$^{-/-}$ mice. Table S1 summarizes the primary antibodies used for immunofluorescence. Online supplemental material is available at http://www.jcb.org/cgi/content/full/jcb.201203065/DC1.

We thank Dr. Masaru Okabe and Ms. Akiko Kawai for supporting the generation of the *Qbrick*^{RGE} mice. We thank Dr. Yoshikazu Sado for anti–mouse type IV collagen monoclonal antibodies, Dr. Ryoko Sato-Nishiuchi for the anti-Velcro polyclonal antibody, and Ms. Noriko Sanzen for anti–mouse laminin monoclonal antibodies.

This study was supported by the Grant-in-Aid for Scientific Research on Priority Areas (#17082005) and the Grant-in-Aid for Scientific Research on Innovative Areas (#22122006) from the Ministry of Education, Culture, Sports, Science and Technology of Japan.

Submitted: 13 March 2012
Accepted: 25 April 2012

References

Abramoff, M.D., P.J. Magalhaes, and S.J. Ram. 2004. Image Processing with ImageJ. *Biophotonics International*. 11:36–42.

Alazami, A.M., R. Shaheen, F. Alzahrani, K. Snape, A. Saggar, B. Brinkmann, P. Bavi, L.I. Al-Gazali, and F.S. Alkuraya. 2009. *FREM1* mutations cause bifid nose, renal agenesis, and anorectal malformations syndrome. *Am. J. Hum. Genet.* 85:414–418. http://dx.doi.org/10.1016/j.ajhg.2009.08.010

Bladt, F., A. Tafuri, S. Gelkop, L. Langille, and T. Pawson. 2002. Epidermolysis bullosa and embryonic lethality in mice lacking the multi-PDZ domain protein GRIP1. *Proc. Natl. Acad. Sci. USA*. 99:6816–6821. http://dx.doi.org/10.1073/pnas.092130099

Boyd, P.A., J.W. Keeling, and R.H. Lindenbaum. 1988. Fraser syndrome (cryptophthalmos-syndactyly syndrome): a review of eleven cases with postmortem findings. *Am. J. Med. Genet.* 31:159–168. http://dx.doi.org/10.1002/ajmg.1320310119

Brandenberger, R., A. Schmidt, J. Linton, D. Wang, C. Backus, S. Denda, U. Müller, and L.F. Reichardt. 2001. Identification and characterization of a novel extracellular matrix protein nephronectin that is associated with integrin α8β1 in the embryonic kidney. *J. Cell Biol.* 154:447–458. http://dx.doi.org/10.1083/jcb.200103069

Carney, T.J., N.M. Feitosa, C. Sonntag, K. Slanchev, J. Kluger, D. Kiyozumi, J.M. Gebauer, J. Coffin Talbot, C.B. Kimmel, K. Sekiguchi, et al. 2010. Genetic analysis of fin development in zebrafish identifies furin and hemicentin1 as potential novel fraser syndrome disease genes. *PLoS Genet.* 6:e1000907. http://dx.doi.org/10.1371/journal.pgen.1000907

Carter, T.C. 1959. Embryology of the Little and Bagg. X-rayed mouse stock. *J. Genet.* 56:401–435. http://dx.doi.org/10.1007/BF02984794

Dalezios, Y., B. Papasozomenos, P. Petrou, and G. Chalepakis. 2007. Ultrastructural localization of Fras1 in the sublamina densa of embryonic epithelial basement membranes. *Arch. Dermatol. Res.* 299:337–343. http://dx.doi.org/10.1007/s00403-007-0763-8

Darling, S., and A. Gossler. 1994. A mouse model for Fraser syndrome? *Clin. Dysmorphol.* 3:91–95. http://dx.doi.org/10.1097/00019605-199404000-00001

Fujiwara, H., M. Ferreira, G. Donati, D.K. Marciano, J.M. Linton, Y. Sato, A. Hartner, K. Sekiguchi, L.F. Reichardt, and F.M. Watt. 2011. The basement membrane of hair follicle stem cells is a muscle cell niche. *Cell*. 144:577–589. http://dx.doi.org/10.1016/j.cell.2011.01.014

Ido, H., A. Nakamura, R. Kobayashi, S. Ito, S. Li, S. Futaki, and K. Sekiguchi. 2007. The requirement of the glutamic acid residue at the third position from the carboxyl termini of the laminin gamma chains in integrin binding by laminins. *J. Biol. Chem.* 282:11144–11154. http://dx.doi.org/10.1074/jbc.M609402200

Jadeja, S., I. Smyth, J.E. Pitera, M.S. Taylor, M. van Haelst, E. Bentley, L. McGregor, J. Hopkins, G. Chalepakis, N. Philip, et al. 2005. Identification of a new gene mutated in Fraser syndrome and mouse myelencephalic blebs. *Nat. Genet.* 37:520–525. http://dx.doi.org/10.1038/ng1549

Kiyozumi, D., A. Osada, N. Sugimoto, C.N. Weber, Y. Ono, T. Imai, A. Okada, and K. Sekiguchi. 2005. Identification of a novel cell-adhesive protein spatiotemporally expressed in the basement membrane of mouse developing hair follicle. *Exp. Cell Res.* 306:9–23. http://dx.doi.org/10.1016/j.yexcr.2005.01.020

Kiyozumi, D., N. Sugimoto, and K. Sekiguchi. 2006. Breakdown of the reciprocal stabilization of QBRICK/Frem1, Fras1, and Frem2 at the basement membrane provokes Fraser syndrome-like defects. *Proc. Natl. Acad. Sci. USA*. 103:11981–11986. http://dx.doi.org/10.1073/pnas.0601011103

Linton, J.M., G.R. Martin, and L.F. Reichardt. 2007. The ECM protein nephronectin promotes kidney development via integrin α8β1-mediated stimulation of *Gdnf* expression. *Development*. 134:2501–2509. http://dx.doi.org/10.1242/dev.005033

Manabe, R., K. Tsutsui, T. Yamada, M. Kimura, I. Nakano, C. Shimono, N. Sanzen, Y. Furutani, T. Fukuda, Y. Oguri, et al. 2008. Transcriptome-based systematic identification of extracellular matrix proteins. *Proc. Natl. Acad. Sci. USA*. 105:12849–12854. http://dx.doi.org/10.1073/pnas.0803640105

McGregor, L., V. Makela, S.M. Darling, S. Vrontou, G. Chalepakis, C. Roberts, N. Smart, P. Rutland, N. Prescott, J. Hopkins, et al. 2003. Fraser syndrome and mouse blebbed phenotype caused by mutations in *FRAS1/Fras1* encoding a putative extracellular matrix protein. *Nat. Genet.* 34:203–208. http://dx.doi.org/10.1038/ng1142

Moore, M.W., R.D. Klein, I. Fariñas, H. Sauer, M. Armanini, H. Phillips, L.F. Reichardt, A.M. Ryan, K. Carver-Moore, and A. Rosenthal. 1996. Renal and neuronal abnormalities in mice lacking GDNF. *Nature*. 382:76–79. http://dx.doi.org/10.1038/382076a0

Müller, U., D. Wang, S. Denda, J.J. Meneses, R.A. Pedersen, and L.F. Reichardt. 1997. Integrin α8β1 is critically important for epithelial-mesenchymal interactions during kidney morphogenesis. *Cell*. 88:603–613. http://dx.doi.org/10.1016/S0092-8674(00)81903-0

Nishiuchi, R., J. Takagi, M. Hayashi, H. Ido, Y. Yagi, N. Sanzen, T. Tsuji, M. Yamada, and K. Sekiguchi. 2006. Ligand-binding specificities of laminin-binding integrins: a comprehensive survey of laminin-integrin interactions using recombinant α3β1, α6β1, α7β1 and α6β4 integrins. *Matrix Biol.* 25:189–197. http://dx.doi.org/10.1016/j.matbio.2005.12.001

Osada, A., D. Kiyozumi, K. Tsutsui, Y. Ono, C.N. Weber, N. Sugimoto, T. Imai, A. Okada, and K. Sekiguchi. 2005. Expression of MAEG, a novel basement membrane protein, in mouse hair follicle morphogenesis. *Exp. Cell Res.* 303:148–159. http://dx.doi.org/10.1016/j.yexcr.2004.04.053

Petrou, P., R. Chiotaki, Y. Dalezios, and G. Chalepakis. 2007a. Overlapping and divergent localization of Frem1 and Fras1 and its functional implications during mouse embryonic development. *Exp. Cell Res.* 313:910–920. http://dx.doi.org/10.1016/j.yexcr.2006.12.008

Petrou, P., E. Pavlakis, Y. Dalezios, and G. Chalepakis. 2007b. Basement membrane localization of Frem3 is independent of the Fras1/Frem1/Frem2 protein complex within the sublamina densa. *Matrix Biol.* 26:652–658. http://dx.doi.org/10.1016/j.matbio.2007.05.008

Pichel, J.G., L. Shen, H.Z. Sheng, A.C. Granholm, J. Drago, A. Grinberg, E.J. Lee, S.P. Huang, M. Saarma, B.J. Hoffer, et al. 1996. Defects in enteric innervation and kidney development in mice lacking GDNF. *Nature*. 382:73–76. http://dx.doi.org/10.1038/382073a0

Pitera, J.E., P.J. Scambler, and A.S. Woolf. 2008. Fras1, a basement membrane-associated protein mutated in Fraser syndrome, mediates both the initiation of the mammalian kidney and the integrity of renal glomeruli. *Hum. Mol. Genet.* 17:3953–3964. http://dx.doi.org/10.1093/hmg/ddn297

Sánchez, M.P., I. Silos-Santiago, J. Frisén, B. He, S.A. Lira, and M. Barbacid. 1996. Renal agenesis and the absence of enteric neurons in mice lacking GDNF. *Nature*. 382:70–73. http://dx.doi.org/10.1038/382070a0

Sato, Y., T. Uemura, K. Morimitsu, R. Sato-Nishiuchi, R. Manabe, J. Takagi, M. Yamada, and K. Sekiguchi. 2009. Molecular basis of the recognition of nephronectin by integrin α8β1. *J. Biol. Chem.* 284:14524–14536. http://dx.doi.org/10.1074/jbc.M900200200

Slavotinek, A.M., and C.J. Tifft. 2002. Fraser syndrome and cryptophthalmos: review of the diagnostic criteria and evidence for phenotypic modules in complex malformation syndromes. *J. Med. Genet.* 39:623–633. http://dx.doi.org/10.1136/jmg.39.9.623

Smyth, I., X. Du, M.S. Taylor, M.J. Justice, B. Beutler, and I.J. Jackson. 2004. The extracellular matrix gene *Frem1* is essential for the normal adhesion of the embryonic epidermis. *Proc. Natl. Acad. Sci. USA*. 101:13560–13565. http://dx.doi.org/10.1073/pnas.0402760101

Takagi, J., H.P. Erickson, and T.A. Springer. 2001. C-terminal opening mimics 'inside-out' activation of integrin alpha5beta1. *Nat. Struct. Biol.* 8:412–416. http://dx.doi.org/10.1038/87569

Takamiya, K., V. Kostourou, S. Adams, S. Jadeja, G. Chalepakis, P.J. Scambler, R.L. Huganir, and R.H. Adams. 2004. A direct functional link between the multi-PDZ domain protein GRIP1 and the Fraser syndrome protein Fras1. *Nat. Genet.* 36:172–177. http://dx.doi.org/10.1038/ng1292

Timmer, J.R., T.W. Mak, K. Manova, K.V. Anderson, and L. Niswander. 2005. Tissue morphogenesis and vascular stability require the Frem2 protein, product of the mouse myelencephalic blebs gene. *Proc. Natl. Acad. Sci. USA*. 102:11746–11750. http://dx.doi.org/10.1073/pnas.0505404102

Vrontou, S., P. Petrou, B.I. Meyer, V.K. Galanopoulos, K. Imai, M. Yanagi, K. Chowdhury, P.J. Scambler, and G. Chalepakis. 2003. *Fras1* deficiency results in cryptophthalmos, renal agenesis and blebbed phenotype in mice. *Nat. Genet.* 34:209–214. http://dx.doi.org/10.1038/ng1168

Kiyozumi et al., http://www.jcb.org/cgi/content/full/jcb.201203065/DC1

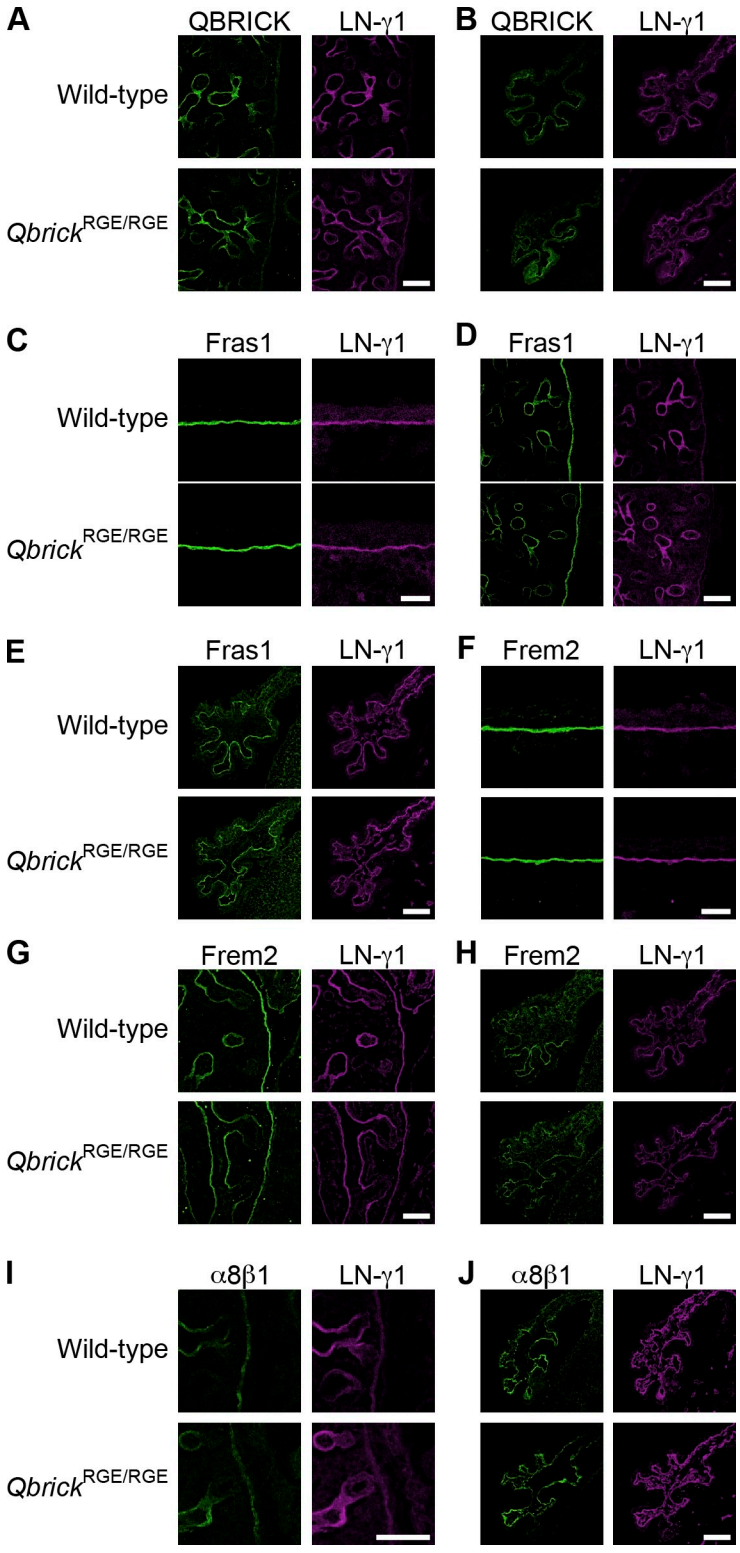

Figure S1. **Expression of FS-associated proteins and in situ binding of integrin α8β1 at the BMs of *Qbrick*$^{RGE/RGE}$ embryos.** Immunofluorescence staining (green) for QBRICK (A and B), Fras1 (C–E), Frem2 (F–H), and exogenously added integrin α8β1 (I and J) at the BMs of the lung (A, D, G, and I), choroid plexus (B, E, H, and J), and skin (C and F) of E15.5 *Qbrick*$^{RGE/RGE}$ embryos. Laminin-γ1 immunofluorescence staining (magenta) to visualize the BMs is also shown. In each set of panels, the top and bottom panels show fluorescence images for wild-type and *Qbrick*$^{RGE/RGE}$ littermates, respectively. Bars: (A, B, D, E, and G–J) 100 µm; (C and F) 20 µm.

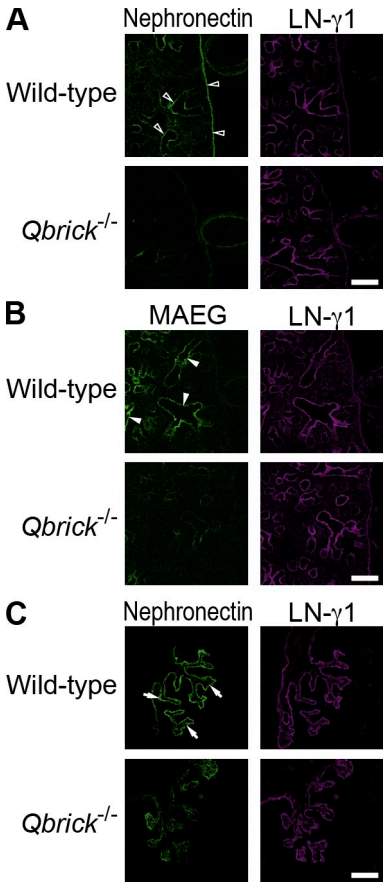

Figure S2. **Impaired expression of nephronectin and MAEG in *Qbrick*$^{-/-}$ mice.** The left panels show immunofluorescence staining (green) for nephronectin (A and C) and MAEG (B) in the E15.5 developing lung (A and B) and choroid plexus (C). The right panels show laminin-γ1 immunofluorescence staining (magenta) to visualize the BMs. In each set of panels, the top and bottom panels show fluorescence images for wild-type and *Qbrick*$^{-/-}$ littermates, respectively. In the E15.5 lung, the expression of nephronectin is high at the BMs of the pleura and lung epithelia in wild-type embryos (open arrowheads), but is greatly diminished in the *Qbrick*$^{-/-}$ littermates. Similarly, the expression of MAEG, which is high at the lung epithelial BMs in wild-type embryos (closed arrowheads), is greatly diminished in the *Qbrick*$^{-/-}$ littermates. In the E15.5 choroid plexus, the expression of nephronectin is high at the ependymal BM in wild-type embryos (arrows), but is considerably attenuated in the *Qbrick*$^{-/-}$ littermates. Bars, 100 µm.

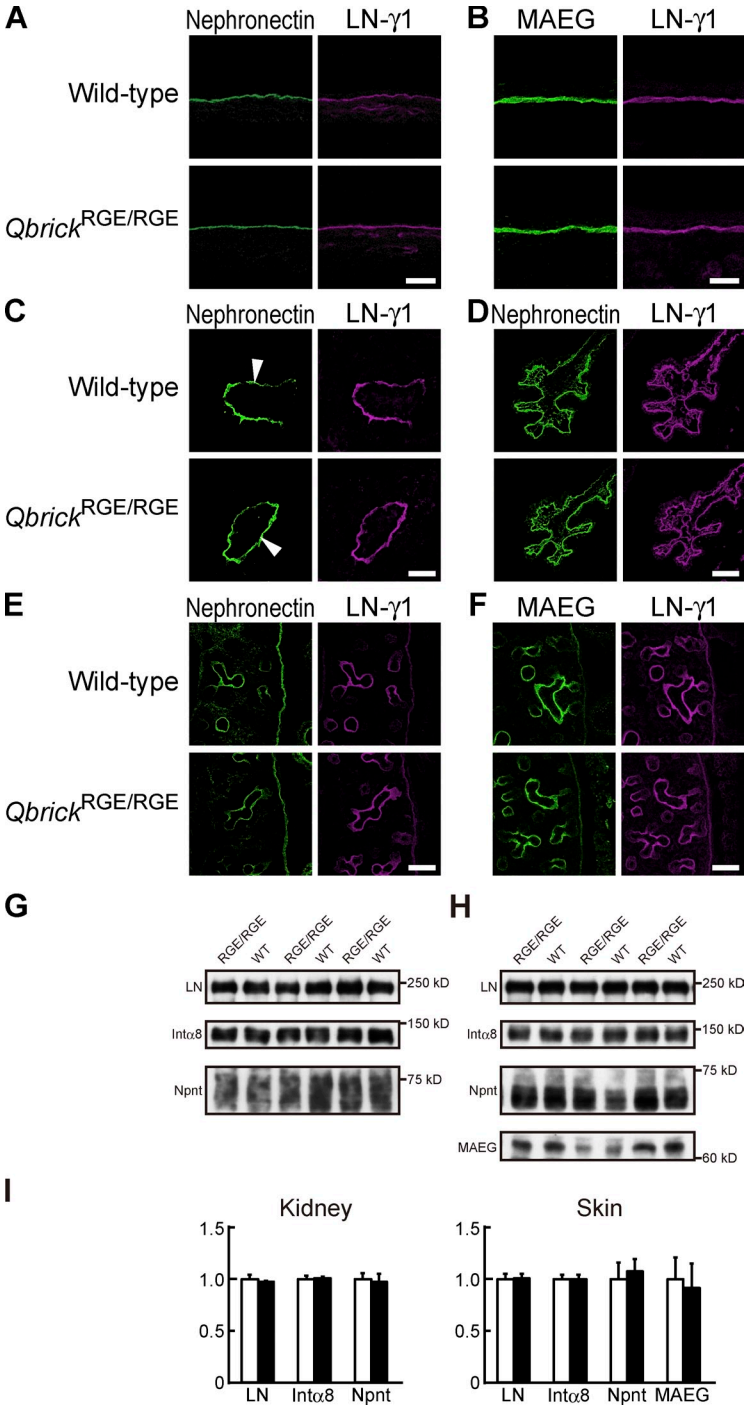

Figure S3. **Expression of nephronectin and MAEG in *Qbrick*$^{RGE/RGE}$ embryos.** The left panels show immunofluorescence staining (green) for nephronectin (A and C–E) and MAEG (B and F) in the E15.5 skin (A and B), E11.5 ureteric bud (C), E15.5 choroid plexus (D), and E15.5 lung (E and F). The right panels show laminin-γ1 immunofluorescence staining (magenta) to visualize the BMs. In each set of panels, the top and bottom panels show fluorescence images for wild-type and *Qbrick*$^{RGE/RGE}$ littermates, respectively. Bars: (A and B) 20 μm; (C–F) 100 μm. (G and H) Immunoblot detection of laminin β1 and γ1 chains (LN), integrin α8 (Intα8), nephronectin (Npnt), and MAEG in protein extracts from the kidney (G) and skin (H) of E15.5 *Qbrick*$^{RGE/RGE}$ mice and their wild-type littermates. (I) Immunoblot signal intensities of laminin β1 and γ1 chains (LN), integrin α8 (Intα8), nephronectin (Npnt), and MAEG in the kidney and skin of E15.5 wild-type (open bars) and *Qbrick*$^{RGE/RGE}$ (shaded bars) mice. The signal levels in control mice were set at 1. Each bar represents the mean ± SD (error bars; $n = 3$).

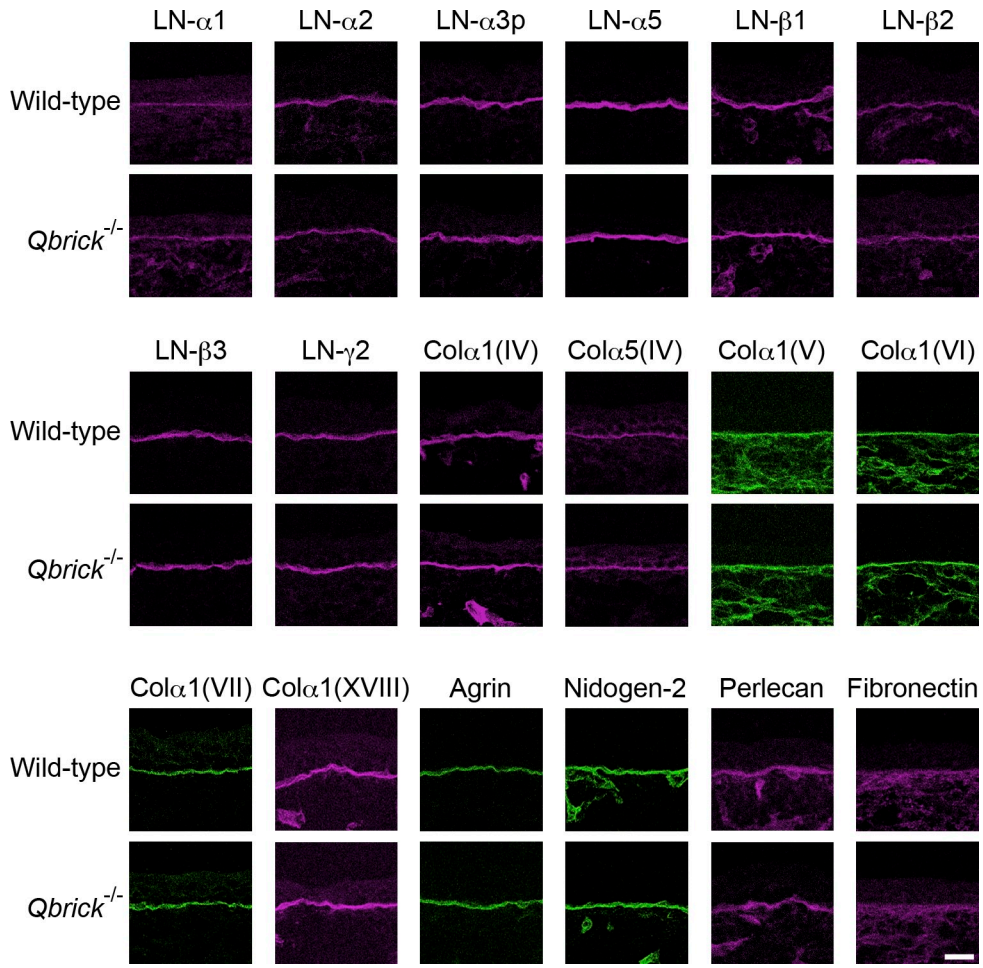

Figure S4. **Expression of various BM proteins in *Qbrick*$^{-/-}$ mice.** The expression of BM proteins was investigated by immunofluorescence staining of the E15.5 dorsal skin. In each set of panels, the top and bottom panels show fluorescence images for wild-type and *Qbrick*$^{-/-}$ littermates, respectively. Bar, 20 µm.

Table S1. **Antibodies used for immunofluorescence staining**

Antibody	Company/reference	Concentration/dilution
Laminin-α1	Manabe et al., 2008	0.5 µg/ml
Laminin-α2	Manabe et al., 2008	1.5 µg/ml
Laminin-α3p	Manabe et al., 2008	0.25 µg/ml
Laminin-α5	Manabe et al., 2008	0.25 µg/ml
Laminin-β1	Manabe et al., 2008	0.3 µg/ml
Laminin-β2	Manabe et al., 2008	0.6 µg/ml
Laminin-β3	Manabe et al., 2008	0.2 µg/ml
Laminin-γ1	Millipore	1:2,000
Laminin-γ2	Manabe et al., 2008	0.9 µg/ml
Collagen α1 (IV)	Sado et al., 1995	1:1500
Collagen α5 (IV)	Seki et al., 1998	1:500
Collagen α1 (V)	LSL	1:10,000
Collagen α1 (VI)	Rockland Immunochemicals	1:50,000
Collagen α1 (VII)	EMD	1:1,000
Collagen XVIII	R&D Systems	1:4,000
Agrin	Manabe et al., 2008	1:1500
Nidogen-2	Manabe et al., 2008	0.2 µg/ml
Perlecan	Millipore	1:1,000
Fibronectin	Sekiguchi et al., 1985	1 µg/ml
Nephronectin	Manabe et al., 2008	1 µg/ml
MAEG	Osada et al., 2005	3 µg/ml
QBRICK	Kiyozumi et al., 2005	3 µg/ml
Fras1	Kiyozumi et al., 2006	3 µg/ml
Frem2	Kiyozumi et al., 2006	3 µg/ml

References

Kiyozumi, D., A. Osada, N. Sugimoto, C.N. Weber, Y. Ono, T. Imai, A. Okada, and K. Sekiguchi. 2005. Identification of a novel cell-adhesive protein spatiotemporally expressed in the basement membrane of mouse developing hair follicle. *Exp. Cell Res.* 306:9–23. http://dx.doi.org/10.1016/j.yexcr.2005.01.020

Kiyozumi, D., N. Sugimoto, and K. Sekiguchi. 2006. Breakdown of the reciprocal stabilization of QBRICK/Frem1, Fras1, and Frem2 at the basement membrane provokes Fraser syndrome-like defects. *Proc. Natl. Acad. Sci. USA.* 103:11981–11986. http://dx.doi.org/10.1073/pnas.0601011103

Manabe, R., K. Tsutsui, T. Yamada, M. Kimura, I. Nakano, C. Shimono, N. Sanzen, Y. Furutani, T. Fukuda, Y. Oguri, et al. 2008. Transcriptome-based systematic identification of extracellular matrix proteins. *Proc. Natl. Acad. Sci. USA.* 105:12849–12854. http://dx.doi.org/10.1073/pnas.0803640105

Osada, A., D. Kiyozumi, K. Tsutsui, Y. Ono, C.N. Weber, N. Sugimoto, T. Imai, A. Okada, and K. Sekiguchi. 2005. Expression of MAEG, a novel basement membrane protein, in mouse hair follicle morphogenesis. *Exp. Cell Res.* 303:148–159. http://dx.doi.org/10.1016/j.yexcr.2004.04.053

Sado, Y., M. Kagawa, Y. Kishiro, K. Sugihara, I. Naito, J.M. Seyer, M. Sugimoto, T. Oohashi, and Y. Ninomiya. 1995. Establishment by the rat lymph node method of epitope-defined monoclonal antibodies recognizing the six different alpha chains of human type IV collagen. *Histochem. Cell Biol.* 104:267–275. http://dx.doi.org/10.1007/BF01464322

Seki, T., I. Naito, T. Oohashi, Y. Sado, and Y. Ninomiya. 1998. Differential expression of type IV collagen isoforms, α5(IV) and α6(IV) chains, in basement membranes surrounding smooth muscle cells. *Histochem. Cell Biol.* 110:359–366. http://dx.doi.org/10.1007/s004180050296

Sekiguchi, K., A. Siri, L. Zardi, and S. Hakomori. 1985. Differences in domain structure between human fibronectins isolated from plasma and from culture supernatants of normal and transformed fibroblasts. Studies with domain-specific antibodies. *J. Biol. Chem.* 260:5105–5114.